A Multiomic Analysis Reveals How Breast Cancers Disseminated to the Bone Marrow Acquire Aggressive Phenotypes through Tumor-Stroma Tunnels

Authors and affiliations

Saptarshi Sinha[1], Brennan W. Callow[2], Alex P. Farfel[2], Suchismita Roy[1], Siyi Chen[2], Shrila Rajendran[2], Johanna M. Buschhaus[2,3], Kathryn E. Luker[2,4], Pradipta Ghosh[1,5,6,7*], Gary D. Luker[2,3,4,8*]

[1]Department of Cellular and Molecular Medicine, School of Medicine, University of California San Diego, La Jolla, CA, USA

[2] Center for Molecular Imaging, Department of Radiology, University of Michigan, Ann Arbor, MI, USA

[3]Department of Biomedical Engineering, University of Michigan, Ann Arbor, MI, USA

[4]Biointerfaces Institute, University of Michigan, Ann Arbor, MI, USA

[5]Moores Comprehensive Cancer Center, [6]Department of Medicine, [7]School of Medicine, and Veterans Affairs Medical Center, University of University of California San Diego, La Jolla, CA

[8]Department of Microbiology and Immunology, University of Michigan, Ann Arbor, MI, 48109-2200, USA

*Corresponding authors:

Pradipta Ghosh, M.D.; Professor, Departments of Medicine and Cellular and Molecular Medicine, University of California San Diego, 9500 Gilman Drive (MC 0651), George E. Palade Bldg, Rm 232, 239, La Jolla, CA 92093; Phone: 858-822-7633. Email: prghosh@ucsd.edu

Gary D. Luker, M.D.; Professor, Radiology, Biomedical Engineering, and Microbiology and Immunology, A524 BSRB, 109 Zina Pitcher Place, Ann Arbor, MI 48109-2200. Phone: 734-764-2890. Email: gluker@umich.edu

Running title

GIV borrowed through nanotubes drives aggressive disease in ER+ breast cancer

Key Words

Connexons; Mesenchymal stem cells; Tunneling nanotubes; Metastasis; Bone Marrow; Girdin

Abstract

Estrogen receptor-positive (ER+) breast cancer commonly disseminates to bone marrow, where interactions with mesenchymal stromal cells (MSCs) shape disease trajectory. We modeled these interactions with tumor-MSC co-cultures and used an integrated transcriptome-proteome-network-analyses workflow to identify a comprehensive catalog of contact-induced changes. Induced genes and proteins in cancer cells, some borrowed and others tumor-intrinsic, were not recapitulated merely by conditioned media from MSCs. Protein-protein interaction networks revealed the rich connectome between 'borrowed' and 'intrinsic' components. Bioinformatic approaches prioritized one of the 'borrowed' components, *CCDC88A*/GIV, a multi-modular metastasis-related protein which has recently been implicated in driving one of the hallmarks of cancers, i.e., growth signaling autonomy. MSCs transferred GIV protein to ER+ breast cancer cells (that lack GIV) through tunnelling nanotubes via connexin (Cx)43-facilitated intercellular transport. Reinstating GIV alone in GIV-negative breast cancer cells reproduced ~20% of both the 'borrowed' and the 'intrinsic' gene induction patterns from contact co-cultures; conferred resistance to anti-estrogen drugs; and enhanced tumor dissemination. Findings provide a multiomic insight into MSC→tumor cell intercellular transport and validate how transport of one such candidate, GIV, from the haves (MSCs) to have-nots (ER+ breast cancer) orchestrates aggressive disease states.

GRAPHIC ABSTRACT

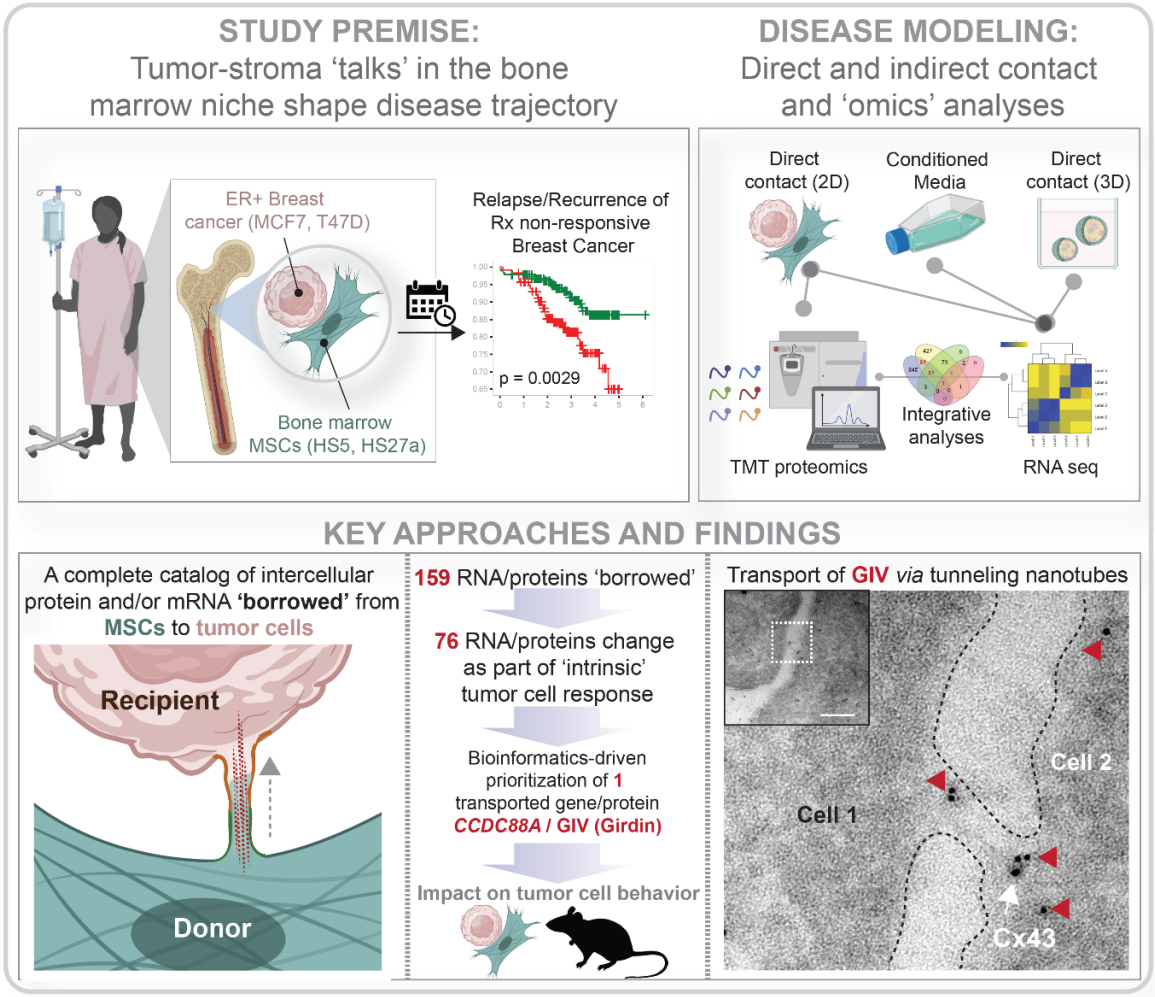

Introduction

Estrogen receptor-positive (ER+) breast cancer, the most common subtype, preferentially disseminates to bone and bone marrow(1, 2). Bone metastases are incurable, and cause debilitating symptoms, e.g., pain, fractures, and life-threatening hypercalcemia(3). The bone marrow, on the other hand, harbors disseminated tumor cells (DTCs) in breast cancer; DTCs may persist in a clinically occult state for decades before they may ultimately proliferate and potentially travel to other organs to produce delayed recurrences that occur in ~40% of patients with ER+ breast cancer(4). Recurrent disease is more aggressive, relatively resistant to treatment, and currently incurable. Little progress has been made in treating breast cancer that has already disseminated to bone(5), largely because we lack a comprehensive understanding of the molecular mechanisms that make ER+ breast cancer cells more aggressive in the bone marrow niche(6).

What is widely believed is that interactions with stromal cells in the bone marrow environment shape key functions of breast cancer cells that ultimately determine disease progression and outcomes(7). Mesenchymal stem cells (MSCs), a multipotent cell type that contributes to formation of bone, fat, and cartilage tissues, are a major stromal cell type driving aggressive phenotypes of disseminated ER+ breast cancer cells in bone marrow. MSCs regulate ER+ breast cancer cells through mechanisms such as secreted cytokines and direct intercellular interactions(8). Work by us and others have established that direct interactions with MSCs, rather than soluble molecules, drive changes in gene expression and metabolism that promote cancer stem-like cell states, resistance to anti-estrogen drugs, and metastasis in ER+ breast cancer(9-11). Breast cancer cells and MSCs are known to establish channels of intercellular communication that transport molecules and organelles. The two major structures for such intercellular communication include: Gap junctions and tunneling nanotubes (TNTs), both of which share connexin 43 (Cx43) as an essential molecular player. Gap junctions are intercellular channels comprised of various subsets of connexin proteins(12). Gap junctions and Cx43 are upregulated in lymph node and systemic metastases in breast cancer and other malignancies, suggesting these structures contribute to essential steps in the metastatic cascade(13). TNTs are actin-rich long, thin tubes that may form between cells of the same or different types, thereby allowing long-range communication via the exchange of materials. A broad range of intracellular contents, including microRNAs, proteins, and organelles, exchange between cells via TNTs. TNTs increase drug resistance of cancer cells; regulate proliferation; and promote metastasis.

Despite these insights, a limited number of molecules transferred from MSCs via gap junctions or TNTs have been implicated in aggressive phenotypes of breast cancer cells, whereas the identity of most remains unknown. Here we tackle this knowledge gap by performing a comprehensive multiomic network analysis to identify molecules and biologic processes regulated by direct contact between bone marrow MSCs and ER+ breast cancer cells. We identified genes and proteins that cancer cells acquire from MSCs through direct transfer ("borrowed" components) and additional molecules they induce because of such transfer ("intrinsic components"). We use bioinformatic

approaches to explore the implications of these gene expression changes on patient outcome and subsequently prioritized one 'borrowed' gene/protein (*CCDC88A/*GIV) to explore further and validate through a series of *in vitro* and *in vivo* studies. Our findings establish a comprehensive resource for changes induced in ER+ breast cancer cells by contact with bone marrow MSCs and pinpoint GIV as a promising target to overcome aggressive phenotypes that breast cancer cells acquire in a bone marrow environment.

Results

Multiomic analysis of the impact of close contact between ER+ breast cancer cells and MSCs

DTCs in the bone marrow displace hematopoietic stem cells from supportive niches(14), where they establish direct contact with various subsets of MSCs and eventually gain aggressiveness. To identify how MSCs may impact ER+ breast cancer cells through direct contact, we used a 2D co-culture model combining MCF7 or T47D human ER+ breast cancer cells with human HS5 or HS27a MSCs in a 1:9 ratio (**Fig 1A**). After 3 days of co-culture in medium with low serum and physiologic concentrations of glucose, we recovered the tumor cells using EpCAM immunomagnetic beads, capitalizing on the fact that EpCAM is expressed exclusively on tumor cells of epithelial origin. We previously showed that such EpCAM-based immunoisolation is relatively devoid of MSC contamination(15). To control for the effects of soluble molecules produced by MSCs, we cultured MCF7 or T47D cells for 3 days in conditioned medium from MSCs (**Fig 1A**). Monocultures of MSCs and tumor cells were used as additional comparator groups. All samples were analyzed by bulk RNA sequencing; mono- and contact cultured MCF7 cells were also analyzed by TMT proteomics.

Exposure of MCF7 cells to contact culture (CC) but not conditioned media (CMed), was associated with a significant lowering of tumor dormancy score (**Fig 1B**); low scores were previously shown to confer a ~2-fold increase in the risk of recurrence in 4 independent cohorts of patients with ER+ breast cancers(16). These findings suggest that our co-culture model captures key transcriptomic changes in ER+ breast cancer cells of translational relevance that correlate with more aggressive disease in patients.

We carried out a combinatorial multiomics analyses to determine what proteins or transcripts may be expressed highly in MSCs that are 'borrowed' by MCF7 cells. To this end, we first created a catalog of genes that are differentially expressed (DEGs; upregulated) in MSCs, but not in MCF7 cells (MCF7 vs HS5; n = 1471; **Fig 1C**). This catalog served as a denominator for all likely candidate genes that a tumor cell may lack originally but acquire from MSCs via intercellular communication. Next, we performed pair-wise DEG analysis on the other MCF7 samples that were subjected to different co-culture conditions. Many genes (n = 482) and proteins (n = 295) were induced due to direct contact culture (CC-induced genes; **Fig 1C**). Few genes were induced because of exposure to conditioned media (CMed-induced genes, n = 13; **Fig 1C**). An overlay of these showed the following: (i) Exposure to conditioned media alone induced only a single unique proteins/transcripts in MCF7 cells, implying soluble mediators or exosomes as potential modes of communication; (ii) By contrast, contact culture could account for 487 unique proteins/transcripts, implying direct contact as the major mode of tumor-MSC communication, accounting for the largest share of the uniquely induced genes; (iii) 242 unique proteins/transcripts (39 transcripts and 203 proteins, with no proteome-transcriptome overlap) were upregulated in MCF7 cells as a consequence of contact culture. These transcripts/proteins were not highly expressed in HS5 cells. This last category was presumed to be tumor cell-intrinsic response to

139 contact culture, unlikely to be transferred directly from MSCs to breast cancer cells. It is noteworthy
140 that neither the experimental design, nor the analytical steps can conclude with certainty if transport
141 of a given target occurred as a protein or as mRNA because unknown factors (transcript/protein half-
142 life) are expected to confound such conclusions. Similarly, while we infer that 487 unique
143 RNAs/proteins could be transferred during contact culture, i.e., "borrowed" directly by cancer cells
144 from the MSCs, we cannot exclude some cancer cell-intrinsic contributions to the overall levels. We
145 did observe, however, that the 'borrowed' RNA/proteins were enriched for biological processes that
146 govern tube morphogenesis, organization of extracellular encapsulated structures, and movement of
147 anatomic structures in the context of multicellular systems (**Fig 1D**). Enrichment of these processes
148 further suggests the potential for direct transfer of RNA/protein from MSCs to cancer cells through
149 structures such as tunneling nanotubes. Reactome and gene ontology analyses of the genes induced
150 by conditioned media, contact culture and intrinsic response present a comprehensive picture of
151 distinct modes by which MSCs shape behavior and function of cancer cells (**Supplementary Fig 2**).
152 A similar analysis for the transcripts and proteins that were downregulated during contact culture and
153 when exposed to conditioned media was notable for genes/proteins that reduce the dependence on
154 ER signaling (**Supplemental Fig 1**). A full catalog of all the genes/proteins that are upregulated
155 (**Supplemental information 1**) and downregulated (**Supplemental information 2**) during contact
156 culture are provided.
157
158 **A gene signature of contact culture is prognostic and predictive in ER+ breast cancers.**
159 We noted that 39 unique genes were upregulated, identified by both RNA seq and TMT proteomics,
160 in MCF7 cells during contact co-cultures (**Fig 1C**). Almost all of them (n=38; **Fig 1E**) were uniquely
161 upregulated during contact culture, whereas 1 (*KYNU*) was upregulated in conditioned media. A
162 heatmap analysis showed that these 39 genes are poorly expressed in monocultured MCF7 cells
163 (MC; **Fig 1E**) but highly expressed in HS5 cells (lane 2; **Fig 1E**). The gene expression patterns in
164 MCF7 cells that were subjected to culture in direct contact with HS5 cells (CC; **Fig 1E**) looked more
165 like that in HS5 cells. By contrast, MCF7 cells subjected to culture in conditioned medium looked
166 virtually indistinguishable from monocultured MCF7 cells (compare MC and CMed; **Fig 1E**). A
167 composite score of the levels of expression of these 39 genes confirmed their statistically significant
168 increase in contact, but not conditioned media cultures (**Fig 1F**). This pattern of gene induction was
169 reproducibly observed when we swapped HS5 in the co-cultures with another MSC line (HS27a; **Fig**
170 **1G**) or swapped the MCF7 tumor cell line with another ER+ breast cancer line (T47D; **Fig 1H**). These
171 findings demonstrate that the 39-gene signature represents a conserved feature of how MSCs impact
172 the properties or behavior of ER+ breast cancer.
173 The 39 genes showed an enrichment of processes that related to growth factor, PI3K/Akt and
174 an *IL4/IL13 and IL10*-centric tolerogenic cytokine signaling (**Fig 2A**), suggesting that the tumor cell's

175 acquisition of these 39 genes from MSCs may impact these aspects of tumor cell biology and/or
176 behavior, including those that concern its interactions with and its ability to evade the immune system.
177 To test its translational relevance, we applied this 39-gene signature to a publicly available
178 dataset that prospectively tracked the outcomes of ER+ breast cancers following neoadjuvant taxane-
179 anthracycline chemotherapy(17) (**Fig 2B-E**). Kaplan-Meier curves revealed that high levels of the
180 contact culture signature correlated with significantly worse distant relapse-free survival in patients
181 with ER+ (**Fig 2B**), but not ER- breast cancers (**Fig 2C**). High levels of the close contact signature
182 also predicted worse outcomes in patients with treatment resistant, but not treatment sensitive,
183 disease (**Fig 2D-E**). Taken together, these findings establish that the 39 genes presumed to be
184 borrowed by ER+ breast cancer cells via direct contact with MSCs carry translationally relevant
185 information; they identify patients at greater risk for death from recurrent breast cancer.
186
187 **The 'borrowed' genes integrate with and intrinsic response during contact culture.**
188 To discover how contact culture with MSCs reprograms signaling networks in ER+ breast cancer
189 cells, we used the 39-proteins as 'seeds' to build a protein-protein interaction (PPI) network (**Fig 3A**).
190 The resultant network (comprised of 2743 proteins) was overlayed with 'borrowed' (n=487) and
191 'intrinsic' (n=242) gene sets (see **Fig 1B**); this allowed construction of a more focused network using
192 159 genes that the ER+ breast cancer cells borrow from MSCs and 76 genes in the cancer cell
193 intrinsic response group. We visualized this network as a multilayer network connecting borrowed
194 (pink; **Fig 3C**) and intrinsic response (green; **Fig 3C**) genes. Within the resultant PPI network, 1482
195 nodes/proteins interacted within 'borrowed' layer and 835 nodes/proteins interacted within the intrinsic
196 layer. The borrowed response interactome was notable for Akt, growth factors and/or their receptors
197 (*EGFR, VEGFA, WNT5A*) and integrins (**Fig 3C**), as noted earlier (**Fig 2A**). Also found in the borrowed
198 network was the gap junction protein, *GJA1*/CX43, which has been implicated in establishment of
199 tunneling nanotubes(18). The two layers shared 567 common nodes/proteins, indicative of
200 meaningful connectivity between the two layers (*p* value of 0.00096, determined by hypergeometric
201 test). The shared nodes were enriched for three prominent themes: membrane trafficking, immune
202 signaling and growth factor signaling (**Fig 3D**).
203 Findings suggest functional integration between the two components; the induction of one (the
204 intrinsic tumor genes) may either enable the functions of and/or reflect the consequences of the other
205 (the borrowed genes). The edge and node list of the entire PPI network, along with its various
206 subnetworks are presented in **Supplemental Information 3**.
207
208 ***CCDC88A*/GIV as a key gene borrowed by cancer cells amidst robust intercellular transport**
209 With an intent to validate and/or characterize key components of the borrowed
210 proteome/transcriptome, we further refined the list of borrowed genes derived in our 2D contact
211 culture model (**Fig 1A**) leveraging a previously published 3D contact culture of MCF7 or T47D cells

212 with HS5 (**Fig 3E**)(19). Such a refinement was carried out with a two-fold intention: (i) to enhance the
213 physiological context and translational relevance because TNTs have been shown to be formed in
214 3D culture systems(20); and (ii) to provide a continuity between 2D and 3D TNT biology, which has
215 been a difficult task to achieve in a field that is still in its infancy(21). Refinement gave a handful genes
216 (n=19) that are induced also during 3D close contact culture in both MCF7 and T47D cells (**Fig 3F**).
217 Gene ontology (GO) analysis of these 19 genes revealed that one gene, *CCDC88A* [which encodes
218 the protein Gα-Interacting, Vesicle-associated (GIV, a.k.a, Girdin)] is commonly shared among all key
219 processes upregulated in ER+ breast cells by contact with MSCs (**Fig 3G**). Compared to
220 monocultured *CCDC88A* transcript was significantly upregulated in our 2D direct contact but not the
221 conditioned medium cultured MCF7 cells (**Fig 3H**). A focused analysis of the *CCDC88A/GIV*-
222 subnetwork from the multi-layer interactome (in **Fig 3C**) revealed that the interactome of GIV could
223 support numerous pathways and processes involved in cell projections and membrane domains (**Fig**
224 **3I**), suggesting that *CCDC88A* associates with direct intercellular contacts.
225 We confirmed by interferometry microscopy that 'borrowing' of *CCDC88A* in our 2D contact
226 culture system (**Fig 3H**) was associated with the presence of numerous TNTs connecting MCF7 and
227 HS5 cells (**Fig 3J**, **Supplementary Figure 3**). TNT formation in contact cultures was associated also
228 with the elevated expression of two proteins previously implicated as central factors for TNT formation:
229 (i) the gap junction protein *GJA1* (18)(connexin 43, CX43; **Fig 3K**) and the TNT marker, *TNFAIP2*
230 (22)(M-Sec; **Fig 3L**). To investigate if gap-junction or TNT-facilitated intercellular communication is
231 functional (i.e., allowed intercellular communication) we carried out the well-established calcein-AM
232 transfer assay(23, 24). When MCF7 cells that stably expressed mCherry (recipients) were cocultured
233 with calcein-labeled HS5 MSCs (donors) or Calcein-labeled MCF7 cells, we detected the successful
234 transfer of calcein into mCherry-labeled MCF7 cells (**Supplementary Figure 4**). While both donor
235 cells (HS5 and MCF7 cells) transferred calcein to the recipient MCF7 cells, transfer was markedly
236 more from HS5 cells (**Supplementary Figure 4**). These results confirm that our 2D contact cultures
237 were permissive to intercellular transport.
238 Together these findings suggest that TNTs in contact cultures could serve as a route for breast
239 cancer cells to borrow from MSCs certain RNAs and proteins, among which, *CCDC88A*/GIV may be
240 a central player.
241
242 **GIV(*CCDC88A*) is transported from MSCs to ER+ breast cancer cells**
243 Although GIV was prioritized through computational rationale (**Fig 3E-I**), we prioritized its candidacy
244 for further validation as opposed to any of the other 18/19 candidate genes (**Fig 3F**) because of three
245 key reasons: *First*, as a large multi-modular protein shown to integrate signals initiated by diverse
246 classes of receptors and those transduced through diverse signaling pathways, GIV has been
247 implicated in tumor cell aggressiveness (stemness(25), survival after DNA damage(26),
248 invasiveness(26), chemoresistance(27) and acquisition of metastatic potential(28)) by diverse groups

249 in a multitude of cancers, including breast(29) and is considered to be a metastasis-related
250 protein(30). *Second*, unlike stromal cells(31, 32) and triple negative breast cancers, which express
251 high levels of GIV, ER+ breast cancer cells, such as MCF7 and T47D, have been shown to be GIV-
252 deficient(33) due to an alternative splicing event [intron 19 retention], which leads to the loss of the
253 resultant transcript to non-sense mediated decay. The concept of haves (MSCs) lending GIV to have
254 nots (ER+ tumor cells) for a potential gain in metastatic potential by the latter appeared interesting.
255 Consistent with this concept, prior studies had in fact demonstrated that patients with ER+ breast
256 cancers do express GIV, and such expression correlates with more metastasis and poorer
257 survival(34, 35). *Third*, GIV has recently been shown to be a key orchestrator of secretion-coupled
258 autonomy(36), wherein cancer cells may secrete and sense their own growth factors to survive.
259 Proteomic studies confirmed that GIV enabled autocrine growth factor signaling autonomy specifically
260 within the EGF/EGFR system(36). It is noteworthy that EGFR is one of the initially identified list of 39
261 'borrowed' RNAs and proteins in contact culture (**Fig 1E**). EGFR remained on the list even after the
262 3D contact culture refinement (**Fig 3E**) as one of the 19 "borrowed" genes, alongside *CCDC88A* (**Fig**
263 **3F**).
264 GIV protein was virtually undetectable in the lysates from monocultures of 3 different ER+
265 breast cancer cells but detected as a full-length protein (~250 kDa) in cells recovered with EpCAM-
266 based immunocapture and lysis following 3 days in contact cultures with HS5 cells (**Fig 4B**). GIV
267 protein was detected by immunoblotting in MCF7 cells that were lysed immediately after separation
268 from HS5 cells but not in those after 24 to 96 h of additional culture post separation (**Fig 4C**). These
269 findings indicate that once acquired, GIV is rapidly lost upon returning tumor cells to monoculture,
270 and ongoing close contact with MSCs is essential to maintain the levels of GIV in tumor cells.
271
272 To confirm if GIV in MCF7 cells was indeed acquired from HS5 cells and determine if transport
273 occurred as transcripts or proteins, we stably expressed short hairpin (sh) RNA targeting GIV in either
274 MCF7 or HS5 cells and put them in contact culture with each other in various combinations (see **Fig**
275 **4D**). Batch populations of cells showed ~80% depletion of GIV in HS5 cells (**Fig 4E-***right*). Contact
276 cultures of control MCF7 and HS5 cells showed expected upregulation of both full-length GIV in MCF7
277 cells (**Fig 4E-***left*; lane 3). Contact cultures of MCF7-shGIV cells and HS5 still showed increased
278 amounts of GIV protein, indicating that shRNA against *CCDC88A* did not reduce GIV transfer (**Fig**
279 **4E-***left*; lane 4). However, MCF7 cells co-cultured with HS5-shGIV cells did not result in GIV protein
280 transfer (**Fig 4E-***left*; lane 5). Because MCF7 cells expressing shGIV continued to express GIV
281 protein, findings indicate that the observed upregulation of GIV in MCF7 cells that were subjected to
282 contact culture with HS5 relies predominantly on transfer of GIV as a protein. Some transfer of GIV
283 as mRNA cannot be ruled out.
284
285

286 **Cx43 and GIV interact and are co-transported through intercellular communication sites**
287 Because gap junctions are known to serve as sites for TNT formation and/or attachment(20, 37) and
288 CX43 is a shared molecular entity for them both, we assessed CX43 expression in MCF7 cells that
289 were either in monocultures or recovered from contact cultures with HS5 cells. Co-culture with HS5
290 cells increased CX43 in MCF7 cells, while monocultures of MCF7 cells showed undetectable levels
291 of this protein (**Fig 5A**). Next we used two perturbagens to modulate intercellular communication via
292 gap junctions: (i) Carbenoxolone, a widely used chemical inhibitor of GJIC; and (ii) Fulvestrant, which
293 inhibits the transcriptional functions of ER, and by that token, inhibits various ER targets, including
294 the transcription of CX43(38, 39). Both perturbagens virtually eliminated the upregulation of GIV and
295 CX43 in MCF7 cells co-cultured with HS5 cells (**Fig 5B**), while these compounds had minimal effects
296 on amounts of CX43 in HS5 cells alone (**Supplementary Figure 5**). These results show that direct,
297 CX43-mediated intercellular communication is necessary for MCF7 cells to borrow GIV protein from
298 HS5 cells.
299 To resolve the nature of these CX43-dependent compartments that facilitate intercellular
300 communication, we carried out an ultrastructural analysis by immunogold electron microscopy. CX43
301 and GIV were found to co-localize either near gap junctions (**Fig 5C**-*top left*),at/near more elaborate
302 and less defined contact sites (**Fig 5C**-*bottom left*), or within tube like passages connecting cells (**Fig**
303 **5C**-*right*).
304 Co-localization of CX43 and GIV suggested that these proteins may interact; we asked if they
305 do. Using CX43-GFP expressed in Cos7 cells and purified GST fusions of N-terminal or C-terminal
306 part of GIV in pull down assays, we confirmed that the N-terminus, but not the C-terminus of GIV
307 binds directly to CX43 (**Fig 5D-F**). This finding is consistent with a prior work demonstrating the
308 importance of GIV-NT in junctional localization(40).
309 Together, these findings suggest that CX43 and GIV interact and co-migrate from MSCs to
310 ER+ breast cancer cells during CX43-mediated intercellular transport.
311
312 **Adding GIV to ER+ breast cancer cells recapitulates key functions gained during contact**
313 **culture**
314 Next, we asked what proportion of the functions gained during contact culture with MSCs may be
315 accounted for or recapitulated by GIV alone. To this end, we created MCF7 cells that stably expressed
316 GIV using a piggyBac transposase system (**Fig 6A**) and analyzed them by RNA Seq (**Fig 6B**).
317 Approximately ~20% of the genes in the 'borrowed' (n = 32 genes) and 'intrinsic' response (n = 17
318 genes) components of contact culture were able to perfectly classify the MCF7 cells with or without
319 GIV (**Fig 6C**). A complete catalog of these genes is presented in **Supplemental Information 4**. Heat
320 maps display the differential expression of these genes (**Fig 6E, F**). Of the tumor intrinsic gene
321 response, we previously discovered that co-culture with MSCs upregulated *LCN2,* an iron
322 sequestering protein, and *CD44,* a marker of stem-like cells, in breast cancer cells (15). Pathway

323 analysis of the 32-gene borrowed signature recapitulated by stable expression of GIV alone showed
324 enrichment for numerous processes related to response to external stimuli, while the 17-gene
325 signature included vesicular transport and exocytosis (**Supplemental Figure 6**). These data reinforce
326 our focus on GIV within the list of genes that are transferred from MSCs to breast cancer cells in the
327 bone marrow environment to enhance aggressive traits and facilitate disease progression.

328 To investigate effects of GIV on drug resistance, we focused on anti-estrogen drugs tamoxifen
329 (a selective estrogen receptor modulator)(41) and fulvestrant (a selective estrogen receptor
330 degrader)(42). We also tested combination therapy with fulvestrant and palbociclib, an inhibitor of
331 CDK4/6 used with anti-estrogen therapy for patients with metastatic ER+ breast cancer. Following
332 three days of treatment in low serum, physiologic glucose medium, we quantified relative numbers of
333 viable cells at various concentrations of tamoxifen, fulvestrant, or fulvestrant plus a fixed concentration
334 of palbociclib. MCF7-GIV cells showed resistance to each of these treatment regimens, particularly
335 for fulvestrant (**Fig 6G-I**). These data establish that GIV confers resistance to clinically used drugs for
336 ER+ breast cancer and suggest that upregulation of GIV in cancer cells in close contact with MSCs
337 may permit disseminated ER+ breast cancer cells to survive therapy in the bone marrow environment.

338 Because GIV coordinates intracellular signaling pathways enabling growth-factor autonomous
339 survival and proliferation of circulating tumor cells(36, 43), we investigated the effects of GIV on
340 hematogenous dissemination of ER+ breast cancer cells. We injected MCF7 and MCF7-GIV cells into
341 the left cardiac ventricle of female immunodeficient NOD.Cg-Prkdc scid (NSG) mice and tracked
342 cancer cells using bioluminescence (**Fig 6J**). Viable MCF7 cells dropped significantly and steadily
343 from day 1 through day 10, while the drop was insignificant in mice injected with MCF7-GIV. From
344 days 0-1, signal from control MCF7 cells decreased by approximately 70%, while MCF7-GIV cells
345 diminished by only approximately 10%. From days 1-3, losses of viable cells were approximately 20%
346 and <10% for MCF7 and MCF7-GIV cells, respectively. The rapid drop in MCF7 cells is not
347 unexpected because we did not supplement mice with estrogen, which typically is required for MCF7
348 cells to thrive and proliferate in vivo. Intriguingly, we noted that the differences between groups
349 diminished over time from days 10-24 and became virtually indistinguishable thereafter. These results
350 reveal that GIV facilitates survival during the early stages in dissemination of ER+ breast cancer cells.
351 Because contact culture studies in vitro take ~3 days to transfer GIV, it is possible that MCF7 cells
352 borrowed GIV from stromal cells that have abundant amounts of the same.
353

354 **Tumor cells may acquire *CCDC88A* and other 'borrowed' genes also from fibroblasts**

355 Studies have documented that disseminated tumor cells and metastases in one organ can seed
356 metastatic disease in a second site, emphasizing the need to understand how the bone marrow
357 environment promotes aggressive phenotypes in breast cancer(44). We asked if the usefulness of
358 the catalog of 'borrowed' genes we describe here maintained relevance beyond MSCs and perhaps
359 extend to resident tissue fibroblasts; the latter also are well known to establish TNTs with cancer

360 cells(45). To this end, we leveraged the only publicly available, previously published study that
361 compared monocultures of MCF7 with contact cultures of MCF7 cells and BJ fibroblasts by RNA
362 seq(46). As a third comparator group, they cultured the MCF7 cells in extracellular matrix (ECM) that
363 was derived by concentrating conditioned media from the BJ fibroblasts (CMed) (**Fig 7A**). Contact
364 culture, but not ECM-treated grow conditions induced each of the 3 borrowed gene signatures we
365 described earlier (**Fig 7D-F**). Most importantly, *CCDC88A* was among the "borrowed" gene signature
366 induced during contact culture with fibroblasts. These results suggest that ER+ tumor cells may
367 acquire GIV via intercellular transport from diverse stromal cells, which are known to express GIV at
368 high levels.

Discussion

The major problem we address here is the widely recognized, but poorly understood, means by which the bone marrow environment harbors disseminated tumor cells in ER+ breast cancer, permitting long-term survival of these cells despite hormone targeted therapy(47). Persistence of disseminated tumor cells poses a documented, progressively increasing risk of delayed recurrence that most often occurs in bone (48-50) (~50%) for patients with ER+ breast cancer. MSCs have been implicated as key enablers of tumor cells in the bone marrow niche(51) (52)However, mechanisms that support disseminated tumor cells in bone marrow and potentiate potential recurrence remain unclear. The compendium of TNT tumor-stromal transport we reveal here provides a wealth of potentially actionable targets to disrupt MSC niches for cancer cells and end the current impasse in treating bone metastases. There are potentially three major ways in which this work advances the field of cancer biology.

A catalog of MCS-to-tumor gene transfer

First, we provide here a comprehensive catalog of genes transferred from the MSCs to ER+ breast cancer cells during direct contact culture. The catalog is likely to be physiologically relevant and reproducible because the multiomic rigor we employed went beyond our own datasets generated using all 4 possible combinations of two ER+ breast cancer cell lines and two MSCs. We further refined using datasets from independent laboratories that span both 2D and 3D models. This catalog not only provides a prioritized list of genes for the scientific community to pursue but also provides new knowledge of molecular mechanisms that reprogram breast cancer cells in the bone marrow. For example, while MSCs are known to regulate breast cancer cells through soluble mediators such as cytokines(53), work done by others and us had revealed that key functional changes in ER+ breast cancer cells required direct close contact with MSCs(54). The present catalog provides a new multiomic resource to begin to dissect how MSCs shape disease phenotypes in ER+ breast cancer and to what extent effects rely upon intercellular transfer of key molecules ('borrowed'). We show that the borrowed components integrate seamlessly with a second set of gene expression changes that reflect the cancer cell 'intrinsic' responses; together, they establish a robust connectome. The key borrowed components belong to the growth factor and prosurvival PI3K-Akt signaling pathways. The key intrinsic response is augmentation within the VEGF signaling pathway, which supports proliferation and angiogenesis. The key process suppressed is dependance on estrogen signaling, consistent with environmentally mediated resistance to hormone targeted therapies(55). The 'borrowed' gene signature showed demonstrable translational relevance in that it prognosticated and predicted outcome in patients with ER+ breast cancers, especially in those who had treatment-resistant disease. We conclude that the catalog of genes may represent high value targets for preventing MSCs from empowering tumor cells that lie in the bone marrow niche. Several key genes

406 from this list also were reproducibly upregulated during tumor-fibroblasts contact culture, implying that
407 findings may have broader relevance in the context of tumor cells in other tissue niches.
408
409
410 *Gene transfer occurs through a nanotube-based connectivity grid.*
411 Second, the catalog of genes provides valuable clues into the predominant mode of intercellular
412 communication between MSCs and tumor cells. Intercellular protein transfer encompasses several
413 different biologic processes and cellular structures that establish dynamic communication networks
414 among cells in direct contact or proximity: Gap junctions, TNTs, extracellular vesicles, trogocytosis,
415 and direct cell fusion are among such processes(56). Gene ontology analyses of our catalog of
416 borrowed genes hinted at the formation of extracellular tube-like structures, such as TNTs, as a likely
417 mode of transport. This is consistent with prior reports of MSCs establishing TNTs with multiple types
418 of cancer cells, including MCF7 and other breast cancer cell lines(57). Discovered originally in
419 2004(58), and critiqued initially by some as artifacts of 2D culture(59), TNTs are now increasingly
420 recognized as conduits for cell-cell communication in both physiology and disease(20, 37, 60, 61).
421 They are F-actin rich structures with junctional proteins at one end(62, 63); TNTs couple with adjacent
422 cells through gap junctions(64-67) and both share CX43 as common molecular component. We
423 observed the formation of abundant TNTs connecting MCF7 cells with MSCs and demonstrated that
424 they are functional using pharmacologic inhibitors, implicating gap junctions and CX43 as facilitators
425 of transport in our cultures. The presence of EGFR on the list of 'borrowed' genes is intriguing. While
426 we did not investigate transfer of this receptor as RNA or protein, transmembrane and membrane
427 bound proteins have previously been reported to be transferred via TNTs(68). Most of the borrowed
428 genes, however, represent cytoplasmic proteins and/or organelle- or cytoskeleton-associated
429 proteins, which are known to use TNTs as a route for intercellular protein transfer(20, 37, 61). That
430 the 483 borrowed genes carried an overwhelming message of intercellular transport structures (tube
431 morphogenesis and development) suggests that these genes are selected for their ability to facilitate
432 or support TNT formation, stabilization, and transport. Integration of the borrowed and intrinsic genes
433 through PPI networks indicates that the nature of the exchange is meaningful and advantageous to
434 tumor cells (and potentially also to the MSCs). In doing so, the TNT-dependent tumor-MSC
435 communication we reveal here is resembles the nanotubes(69, 70) and pili-dependent communication
436 in pathogenic biofilm-producing microbes (which are responsible for ~80% of chronic infectious
437 diseases)(71). Unicellular pathogens deploy these structures to communicate with each other, or
438 diverse host cells or other pathogens, to ultimately produce a network of extracellular grid to adopt a
439 'multicellular lifestyle'(72, 73). Such adaptation promotes drug resistance, survival, transfer of
440 resistance genes, metabolic dormancy, in effect, making bacteria difficult to eradicate than when
441 present as unicellular organisms (reviewed in)(74, 75).
442

443 *Acquisition of GIV exemplifies how nanotube-dependent gene transfer benefits cancers*
444 Our bioinformatic analyses pipeline helped prioritize one borrowed gene, *CCDC88A*/GIV, from a list
445 of several interesting candidates. We rationalized it because of its known protumorigenic properties
446 (outlined earlier in *Results*) and because we found it intriguing that the ER+ breast cancer cells
447 typically silence this gene through alternative splicing(33), only to 'borrow' it back from MSCs later in
448 the bone marrow niche (this work). We show that GIV is transferred primarily as protein (not RNA).
449 Because protein transfer is not driven by gradients, and instead relies upon mechanisms of sorting
450 and selective exchange, what governs such selectivity of the borrowed genes remains unclear. In the
451 case of GIV, we show that it binds and co-localizes with CX43 near gap junctions and within TNTs
452 and that the two proteins are co-transferred from MSCs to tumor cells in ways that require functional
453 gap junctions. Discovered originally as an actin binding/remodeling protein in breast cancers(32, 33),
454 and found later to directly bind microtubules and localize to cell junctions under bioenergetic
455 stress(40), both actin and microtubule filaments may serve as highways for transport of GIV between
456 MSCs and tumor cells, as described previously for motor proteins(76) within TNTs. Alternatively,
457 because GIV associates with and regulates the functions and/or the localization of diverse cellular
458 organelles (ERGIC-Golgi vesicles(77), exocytic vesicles(78), endosomes(78, 79),
459 autophagosomes(80)) and of cell surface receptors (e.g., EGFR, integrins, TLR4 etc.)(81), co-
460 transport with such organelles or membrane proteins is also possible. While we did not resolve which
461 of these mechanisms of transfer are at play, we assessed the impact of GIV transfer.
462 By stably expressing GIV alone (among the list of borrowed candidates) in an ER+ breast
463 cancer cell line we recapitulated ~20% of the gene expression patterns within the borrowed and
464 intrinsic response components. Expression of GIV in ER+ breast cancer cells conferred resistance to
465 clinical anti-estrogen drugs and promoted early survival and dissemination of circulating breast cancer
466 cells. *CCDC88A*/GIV is also induced when ER+ tumor cells were placed in contact cultures with
467 fibroblasts, which is in keeping with prior work demonstrating the role of GIV in cancer-associated
468 fibroblasts in the dissemination of cancer(82). Considering the recent revelations that GIV scaffolds
469 a circuit for secretion coupled cellular autonomy (or growth signaling autonomy) in multicellular
470 eukaryotic cells, it is possible that sharing of GIV between haves (stromal cells) and have nots (tumors
471 that are originally GIV-negative) as 'ready-to-use' protein reflects a core biological phenomenon of
472 sharing of resources during an urgent need for survival in growth factor restrictive environments.
473 Transfer as protein bypasses the need for energy expenditure for protein translation and yet achieve
474 higher levels of protein than possible through mRNA transfer; the latter is estimated to be never more
475 than >1% of levels in donor cells(83). Although we found that GIV protein that was acquired during 3
476 days in contact culture was rapidly lost when tumor cells were returned to monoculture, prolonged
477 contact cultures (for months and years, as happens in patients) may allow transferred GIV to initiate
478 the GIV↔STAT3 feedforward loop shown to enhance its own transcription(84). We conclude that

479 intercellular protein transport is a major way for cells to exchange GIV as an essential commodity
480 within a heterotypic population of haves and have nots.
481
482 *Study limitations*
483 A detailed characterization of all that is transported was not pursued. Some genes are likely to be
484 transported from the tumor cells to MSCs; this was not evaluated here. Tolerant immunogenic signals
485 were induced in tumor cells during contact culture; how these signals impact the cancer cell's ability
486 to evade the immune system and/or immune checkpoint blockade therapies will require further studies
487 in humanized mice. TNT-mediated tumor- CAF exchanges are also known to shape tumor cell
488 behaviors(45, 85); dedicated studies are required to further investigate the shared and distinct patters
489 between these (and potentially others, e.g., tumor-myeloid cell) forms of cell-cell communication.
490
491 In conclusion, this work opens new horizons as to how close contact interactions and
492 intercellular communication networks through RNA/protein transfer between ER+ breast cancer cells
493 and MSCs reprograms tumor cells to more aggressive states. Based on the omics-based revelations
494 and experimental evidence (this work) and phenotypic characterization of MSC-tumor contact culture
495 we published earlier(47), we conclude that the TNT-based cell-cell communication in the bone marrow
496 niche (or tumor-stromal or tumor-immune cell communication in any other tissue) may provide the
497 same to tumor cells that nanotube-based communication provides to the bacteria within biofilms; a
498 nutrition- and metabolic stress-free haven to promote sustained survival in new environments.
499 Blocking or redirecting these communication networks, or components transferred through these
500 networks, offers novel opportunities to prevent or cure breast cancer metastasis to bone.

Materials and Methods

Cell culture

We purchased MCF7 (HTB-22) and T47D (HTB-133) human ER+ breast cancer cell lines, Cos7 cells, and HS5 (CRL-11882) and HS27a (CRL-2496) human bone marrow MSC line from the American Type Culture Collection (ATCC, Manassas, VA, USA). We thank Dr. James Rae (University of Michigan, Ann Arbor, MI, USA) for providing human HCC1428 ER+ breast cancer cells. We cultured HS5, MCF7, T47D, and Cos7 cells in DMEM (#11995, Gibco, Thermo Fisher, Grand Island, NY, USA) with 10% fetal bovine serum (FBS) (HyClone, ThermoScientific, Waltham, MA, USA), 1% GlutaMAX (#35050, Gibco), and 1% Penicillin-Streptomycin (P/S, #15140, Gibco). We cultured HCC1428 and HS27a cells in RPMI (#11875, Gibco) with 10% FBS, 1% P/S, 1% Sodium Pyruvate (#11360070, Gibco), 1% HEPES (#15630080, Gibco), and 2500 mg/L glucose (#A24940, Gibco). We added 50mg/L Plasmocin™ prophylactic (Invivogen, San Diego, CA, USA) to both DMEM and RPMI media. We maintained cells as previously described (47). We performed mycoplasma testing and authenticated cell lines with short tandem repeats analysis upon initial passaging. We removed cell lines from culture after three months and replaced them with new cells from previously frozen stocks.

Vectors and stable cell lines

We previously described MCF7 cells stably transduced with click beetle green luciferase (MCF7-CBG)(86). For stable RNA interference against GIV, we transduced MCF7 and HS5 cells with shRNA against CCDC88A (clone TRCN0000129915, Millipore Sigma, Burlington, MA, USA), preparing lentiviruses as described previously (87). We used puromycin to select stably transduced cells and performed experiments with batch populations. To stably express full-length GIV in MCF7-CBG cells, we used a PiggyBac transposon with a CAG promoter driving co-expression of GIV and hygromycin linked by a P2A site (VectorBuilder, Chicago, IL, USA). We transfected cells with a 3:1 ratio of GIV transposon to Super PiggyBac Transposase (Systems Biosciences, Palo Alto, CA, USA) using Fugene-HD transfection reagent (Promega, Madison, WI, USA) according to the manufacturer's protocol. Two days after transfection, we selected cells with 150 µg/ml hygromycin B (ThermoFisher, Waltham, MA, USA). After two weeks of culture with hygromycin B, we returned surviving cells to normal growth medium. We transduced MCF7-CBG cells with a lentiviral vector expressing mCherry with a nuclear localization sequence as we reported previously(88).

Co-cultures of breast cancer cells and MSCs

For co-culture assays, we seeded 12,000 total cells per cm^2 in 35 mm dishes with a ratio of 1:9 ER+ breast cancer cells to MSCs. One day after seeding, we washed cells once with phosphate buffered saline (PBS) and then changed medium to phenol-red free DMEM (#A14430-01, Gibco), supplemented with 1% FBS, 1% P/S, 1% Glutamax, 1% sodium pyruvate, 10 nM β-estradiol (#E2758,

538 Sigma-Aldrich, Millipore Sigma, Saint Louis, MO, USA), and 5 mM glucose(89). We cultured cells in
539 low serum (1%), low glucose (4 mM), and 10 nM estrogen (LG/LF) medium for 3 days before
540 analyzing experimental endpoints. We performed assays with conditioned medium as described
541 previously (90).
542
543 **RNA sequencing and differentially expressed gene (DEG) analysis**
544
545 We separated cancer cells from stromal cells with human EpCAM (CD326) immunomagnetic beads
546 (#130-061-101, Miltenyi, Auburn, California, USA) for RNA sequencing as described previously(15).
547 We deposited RNA sequencing data to GEO under accession number GSE224322. Differentially
548 expressed genes from the pairs of experimental conditions are identified using DESeq2 program in
549 R. Genes with log fold change >=2 and a p adjusted value < 0.05 were identified and rank ordered
550 as differentially expressed genes (DEGs) (**Supplemental Information 5**).
551
552 **Hierarchical clustering of RNA seq readouts**
553 Expression patterns of the identified 100 genes that are highly expressed in MCF7 cells post coculture
554 with HS5 cells, are unbiasedly clustered based on their z normalized expression in all the samples
555 using the seaborn clustermap package (v 0.12) in python.
556
557 **Tandem Mass Tag™ (TMT) proteomics and analyses**
558 MCF7 monoculture and post coculture with HS5 cells were subsequently processed for TMT
559 proteomics using LUMOS Orbitrap-Fusion analyzer. Samples were processed at the UC San Diego
560 Biomolecular and Proteomics Mass Spectrometry Core Facility (https://bpmsf.ucsd.edu/). Peptides
561 are identified and mapped using Peaks X Pro pipeline. Intensity ratio of each identified proteins in
562 MCF7 monoculture and post coculture with HS5 cells has been identified and selected if the
563 significance score >20. The mass spectrometry proteomics data have been deposited to the
564 ProteomeXchange Consortium via the PRIDE(91) partner repository with the dataset identifier
565 (**PXD039860**). A list of differentially expressed proteins is provided in **Supplemental Information 6**.
566
567 **StepMiner analysis**
568 StepMiner is an algorithm that identifies step-wise transitions using step function in a time-series
569 data(92). StepMiner undergoes an adaptive regression scheme to verify the best possible up and
570 down steps based on sum-of-square errors. The steps are placed between time points at the sharpest
571 change between expression levels, which gives us the information about timing of the gene
572 expression-switching event. To fit a step function, the algorithm evaluates all possible steps for each
573 position and computes the average of the values on both sides of a step for the constant segments.

An adaptive regression scheme is used that chooses the step positions that minimize the square error with the fitted data. Finally, a regression test statistic is computed as follows:

$$F\ stat = \frac{\sum_{i=1}^{n}(\widehat{X}_i - \bar{X})^2/(m-1)}{\sum_{i=1}^{n}(X_i - \widehat{X}_i)^2/(n-m)}$$

Where X_i for $i = 1$ to n are the values, $\widehat{X}_i$ for $i = 1$ to n are fitted values. m is the degrees of freedom used for the adaptive regression analysis. $\bar{X}$ is the average of all the values: $\bar{X} = \frac{1}{n} * \sum_{j=1}^{n} X_j$. For a step position at k, the fitted values $\widehat{X}_i$ are computed by using $\frac{1}{k} * \sum_{j=1}^{n} X_j$ for $i = 1$ to k and $\frac{1}{(n-k)} * \sum_{j=k+1}^{n} X_j$ for $i = k+1$ to n.

Composite gene signature analysis using Boolean Network Explorer (BoNE)

Boolean network explorer (BoNE)(93) provides an integrated platform for the construction, visualization and querying of a gene expression signature underlying a disease or a biological process in three steps: First, the expression levels of all genes in these datasets were converted to binary values (high or low) using the StepMiner algorithm. Second, Gene expression values were normalized according to a modified Z-score approach centered around *StepMiner* threshold (formula = (expr - SThr)/3*stddev). Third, the normalized expression values for every genes were added together to create the final score for the gene signature. The samples were ordered based on the final signature score. Classification of sample categories using this ordering is measured by ROC-AUC (Receiver Operating Characteristics Area Under The Curve) values. Welch's Two Sample t-test (unpaired, unequal variance (equal_var=False), and unequal sample size) parameters were used to compare the differential signature score in different sample categories. Violin, Swarm and Bubble plots are created using python seaborn package version 0.10.1. Pathway enrichment analyses for genes were carried out via the reactome database (https://reactome.org/) and algorithm(94). Violin plots are created using python seaborn package version 0.10.1.

Survival outcome analyses

Kaplan-Meier (KM) analyses were done for gene signature identified from transcriptome and proteome overlap. The high and low groups were separated based on *StepMiner* threshold on the composite score of the gene expression values. The statistical significance of KM plots was assessed by log rank test. Kaplan-Meier analyses were performed using lifelines python package version 0.14.6.

Flow cytometry for intercellular transfer of calcein, AM

To measure transfer of dye between cells by intercellular connections, we incubated MCF7 or HS5 cells with 10 μM calcein, AM (C3099, Thermo Fisher Scientific) in LG/LF medium for one hour. We then washed cells three times with PBS and seeded labeled MCF7 or HS5 cells with MCF7-mCherry

609 cells at a 9:1 ratio in 10 cm dishes using the cell density described above for co-culture assays. After
610 three days in co-culture, we analyzed amounts of calcein, AM dye in MCF7-mCherry cells by flow
611 cytometry presented as histogram plots.
612
613 **Immunogold electron microscopy**
614 We plated MCF7 monocultures or co-cultures of MCF7 and HS5 cells in 10 cm dishes at densities
615 described above for electron microscopy. After culturing cells for three days in LG/LF medium, we
616 washed cells twice with PBS and then fixed cells with 2% paraformaldehyde and 0.2% glutaraldehyde
617 (#15700 and #16200, respectively, Electron Microscopy Services, Hatfield, PA, USA) for one hour at
618 4°C. We then replaced the solution with ice-cold 4% paraformaldehyde with 0.1% Probumin® BSA in
619 200 mM HEPES and scraped the cells with a soft Teflon scraper (07-200-366, Thermo Fisher). The
620 frozen sample blocks were cryosectioned (60-70 nm thick section 10 µm apart) on EM grid. For
621 immunolabelling, grids were washed with 2% gelatin (cat# ES-006-B; Sigma-Aldrich) in phosphate
622 buffer at 30-37 °C for 15-20 min followed by 10-20 mM (~0.15%) glycine for 5 min and 1% BSA/PBS
623 for 2 min. Grids were incubated with 1:1 anti CX43 antibody (mouse mAb, epitope aa 247-382;
624 BioLegend Cat#850001) and 1:10 anti GIV antibody (Cat#ABT80; Millipore) in 1% BSA/PBS for 1
625 hour at room temperature. For gold labelling the grids were incubated with Goat Anti-Mouse IgG
626 tagged with 12 nm Colloidal Gold (Jackson Immuno research lab cat#115-205-068) and Goat Anti-
627 Rabbit IgG tagged with 6 nm Colloidal Gold (Jackson Immuno research lab cat#111-195-144) diluted
628 in 1:1 in 1% BSA for 1 h at room temperature followed by washing with PBS for 4 times. Then the
629 grids were incubated with 1% Glutaraldehyde in PBS for 5 min. Then the grids were rinsed with
630 distilled water 6 times. For contrast enhancement, the grids were incubated with 2% uranyl acetate
631 at pH 7 for 5 min and in uranyl acetate (4%) (cat# 21447-25; polysciences) and methylcellulose (2%)
632 (cat# 9004-67-5; sigma aldrich) mixture for 5 min. Then the grids were dried in a wire loop at room
633 temperature for 15 min. After that, the grids were mounted in Jeol 1400 plus Transmission Electron
634 Microscope for visualization.
635
636 **Immunoblotting**
637 For immunoblotting in combination with GST pull-down assays (see below), we transfected Cos7 cells
638 with Cx43-GFP (gift from David Spray (Addgene plasmid #69007;
639 http://n2t.net/addgene:69007;RRID:Addgene_69007) (95)) using polyethylenimine (PEI) following the
640 manufacturer's protocol as described in prior work(96, 97). Whole-cell lysates were prepared after
641 washing cells with cold PBS before re-suspending and boiling them in sample buffer. For
642 immunoblotting, protein samples were separated by SDS-PAGE and transferred to polyvinylidene
643 fluoride membranes (Millipore Sigma, MO, USA). The membrane was stained with Ponceau S to
644 visualize proteins Membranes were blocked with PBS supplemented with 5% nonfat milk before
645 incubation with primary antibodies. Infrared imaging with dual-color detection and quantification were

646 performed using a Li-Cor Odyssey imaging system. The anti-CX43 (Biogened, CA, 247-382) antibody
647 was used at 1:1000 v/v dilution. Figures were assembled for presentation using the Photoshop
648 (Adobe, San Jose, CA, USA) and Illustrator (Adobe, San Jose, CA, USA). For co-culture experiments,
649 we separated cancer cells from HS5 cells using EpCAM immunomagnetic beads as described above.
650 We made whole-cell lysates using RIPA lysis buffer and quantified amounts of protein per sample by
651 BCA assay (23235, Thermo Fisher Scientific). We used primary antibodies against GIV (H-6, Santa
652 Cruz Biotechnology, Dallas, TX, USA), CX43 (#3512, Cell Signaling Technology, Danvers, MA, USA),
653 or β-Actin (#4970, Cell Signaling Technology) and detected primary antibodies with appropriate anti-
654 mouse or anti-rabbit secondary antibodies (ThermoFisher) conjugated to horseradish peroxidase. We
655 developed blots with ECL plus reagent (ThermoFisher) and quantified bands using ImageJ.
656
657 **GST pull-down assays**
658 Recombinant GST proteins were expressed in E. coli stain BL21 (DE3) and purified as previously
659 described. Briefly, cultures were induced using 1mM IPTG overnight at 25°C. Cells were then pelleted
660 and resuspended in either GST lysis buffer (25 mM Tris-HCl, pH 7.5, 20 mM NaCl, 1 mM EDTA, 20%
661 (vol/vol) glycerol, 1% (vol/vol) Triton X-100, 2×protease inhibitor cocktail). Recombinant GST alone
662 (control) or GST-tagged GIV proteins, GST-GIV-NT (1-166 aa) and GST-GIV-CT (1660-1870 aa) from
663 *E. coli* were immobilized onto glutathione-Sepharose beads and incubated with binding buffer (50 mM
664 Tris-HCl pH 7.4, 100 mM NaCl, 0.4% (v:v) Nonidet P-40, 10 mM MgCl2, 5 mM EDTA, 2 mM DTT, 1X
665 Complete protease inhibitor) overnight at 4oC temperature. For binding with cell lysates, cells were
666 lysed in cell lysis buffer (20 mM HEPES pH 7.2, 5 mM Mg-acetate, 125 mM K-acetate, 0.4% Triton
667 X-100, 1 mM DTT, 500 μM sodium orthovanadate, phosphatase inhibitor cocktail (Sigma-Aldrich, MO,
668 USA) and protease inhibitor cocktail (Roche Life Science) using a 28G syringe, followed by
669 centrifugation at 10,000Xg for 20 min. Cleared supernatant was then used in binding reaction with
670 immobilized GST-proteins for 4 h at 4°C. After binding, bound complexes were washed four times
671 with 1 ml phosphate wash buffer (4.3 mM Na2HPO4, 1.4 mM KH2PO4, pH 7.4, 137 mM NaCl, 2.7
672 mM KCl, 0.1% (v:v) Tween 20, 10 mM MgCl2, 5 mM EDTA, 2 mM DTT, 0.5 mM sodium
673 orthovanadate). Bound proteins were then eluted through boiling at 100°C in Laemmli sample buffer
674 (BIORAD, CA, USA). The bound proteins were eluted at 37ºC for 10 min.
675
676 **Cell viability assays**
677 For viability assays, we seeded MCF7-CBG or MCF7-CBG-GIV cells at 10,000 cells per well in black
678 wall 96 well plates. We washed cells once PBS and then added various concentrations of tamoxifen,
679 fulvestrant, or fulvestrant with 100 nM palbociclib (all from Cayman Chemical, Ann Arbor, MI, USA) in
680 LG/LF medium with 4 wells per condition. Control wells received vehicle only. After three days in
681 culture, we quantified relative numbers of viable cells by bioluminescence imaging using an IVIS

682 Lumina system with Living Image 4.3.1 software (Perkin Elmer, Waltham, MA, USA) as described
683 previously(47). We plotted data fraction change from vehicle only wells, which we defined as 1.
684
685 **Animal studies**
686 The University of Michigan Institutional Animal Care and Use Committee approved all experiments.
687 We seeded MCF7-CBG or MCF7-CBG-GIV cells in T175 flasks. The following day, we changed
688 medium to LG/LF medium without added estrogen and cultured cells overnight before harvesting cells
689 with cell dissociation buffer (Gibco, ThermoFisher Scientific). We resuspended cells at 1 x 10^5 cells
690 per 100 µl sterile 0.9% NaCl for intracardiac injection. Prior to injection, we verified equal numbers of
691 viable cells based on bioluminescence imaging of aliquots of each cell type. To generate systemic
692 metastases, we injected 1 x 10^5 MCF7-CBG or MCF7-CBG-GIV cells into the left ventricle of 7–10-
693 week-old female NSG mice (7-8 mice per group) (The Jackson Lab, Bar Harbor, ME, USA) as
694 described previously by our lab (89).
695 We performed bioluminescence imaging (IVIS Spectrum, Perkin Elmer) on mice at days
696 indicated in the figure legend. At the end of the study, we measured metastases in defined organs by
697 ex vivo bioluminescence imaging as we reported previously(89). We quantified total bioluminescence
698 signal above background using Living Image software.
699
700 **Study Approval**
701 The University of Michigan IACUC approved all animal procedures under protocol number
702 PRO00010534.
703
704 **Statistics**
705 We performed all cell-based experiments at least three times and presented results as either a
706 representative experiment or average of experiments ± SEM. For statistical analyses, we used
707 python, R, GraphPad Prism software (San Diego, CA, USA) or MATLAB (Mathworks, Natick, MA,
708 USA). $P<0.05$ defined statistical significance for methods listed in figure legends. We assessed
709 statistical significance of Kaplan-Meier plots by log rank test. Kaplan-Meier analyses were performed
710 using lifelines python package version 0.14.6.
711

ACKNOWLEDGEMENTS:

The authors acknowledge funding from United States National Institute of Health grants R01CA238042 (P.G. and G.D.L.); R01CA100768, R01CA160911 (P.G.); R50CA221807 (K.E.L) and U01CA210152, R01CA238023, R33CA225549, and R37CA222563 (G.D.L). We also acknowledge support from the Padres Pedal the Cause #PTC2021 and the Torey Pines Foundation, La Jolla (P.G) and the W.M. Keck Foundation (G.D.L). We thank Guillaume Castillon (UC San Diego Electron Microscopy Core Facility) for technical and logistical support and Debashis Sahoo (UC San Diego) for access to computational platform. This manuscript includes data generated at the UC San Diego Institute of Genomic Medicine (IGM) using an Illumina NovaSeq 6000 that was purchased with funding from a National Institutes of Health SIG grant (#S10 OD026929). The manuscript also includes data generated through the University of Michigan Advanced Genomics, Flow Cytometry, and Pre-Clinical Imaging shared resources supported in part by the University of Michigan Comprehensive Cancer Center support grant P30CA046592.

AUTHOR CONTRIBUTIONS:

S.S, supervised by P.G, carried out and analyzed all electron microscopy, RNA seq, TMT proteomics and computational analyses showcased in this work. Su.R. carried out protein purification and GST pulldown assays. B.W.C, A.P.F., S.C., Sh.R., and J.M.B performed mouse experiments and cell-based assays. K.E.L. provided new reagents. B.W.C. S.S, P.G. and G.D.L. assembled the figures. K.E.L., Su.R., S.S., P.G., and G.D.L. helped write methods and edit the manuscript. G.D.L. and P.G conceptualized, designed, supervised, and analyzed the experiments. K.E.L, S.S. P.G and G.D.L wrote the manuscript. All authors and approved the manuscript prior to submission.

CONFLICT OF INTEREST DISCLOSURE STATEMENT

G.D.L. has received research materials from Spexis. All other authors declare no competing interests.

DATA AVAILABILITY

Data are available via ProteomeXchange with identifier PXD039860 and Gene Expression Omnibus with id GSE224322. The computational analyses can be found at https://github.com/sinha7290/cx43

745 ## FIGURE AND LEGENDS

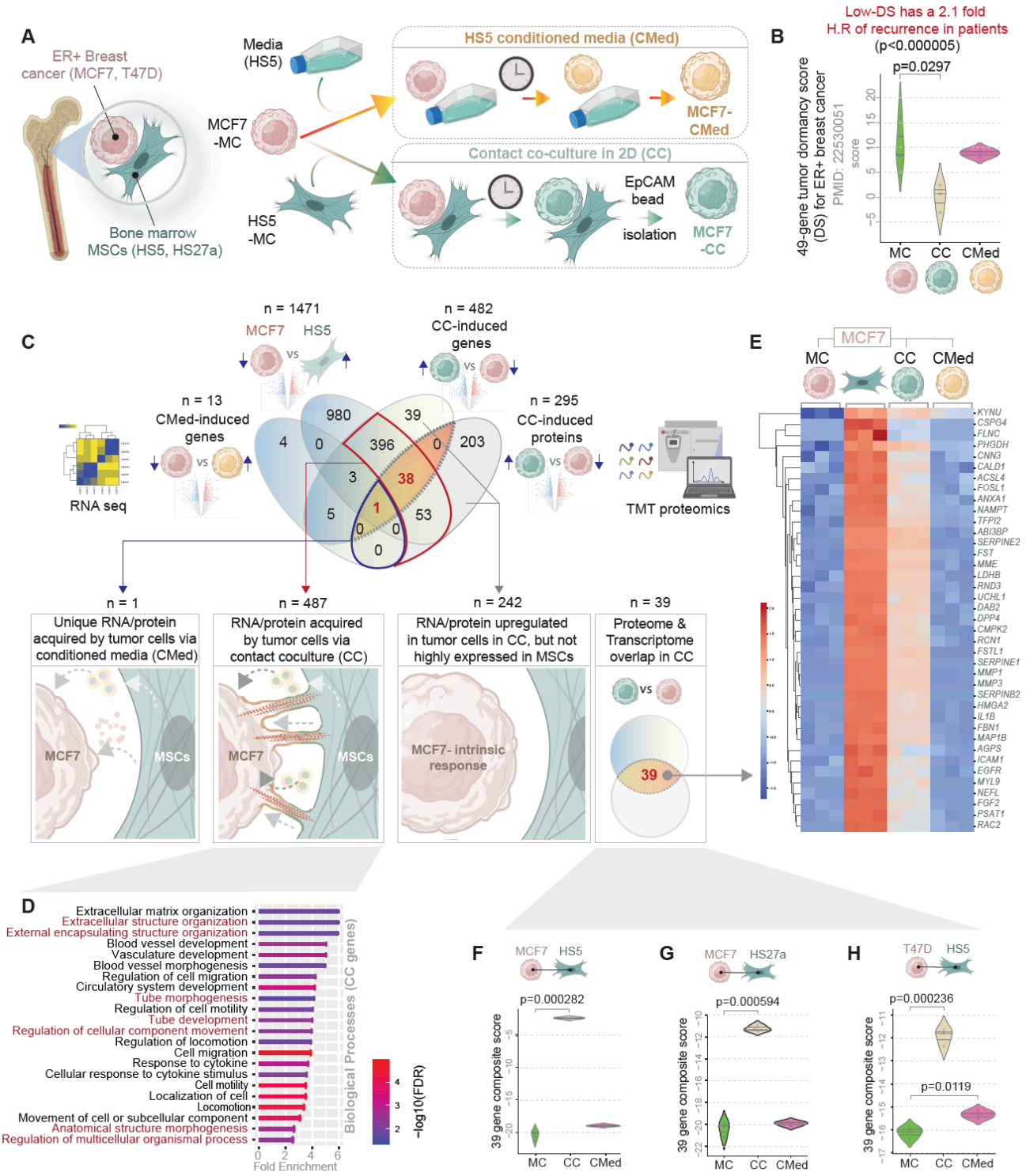

746

747 **Figure 1. Multiomic analysis reveals RNA/protein acquired by ER+ breast cancer cells from**
748 **MSCs in contact coculture.**

749 **A**. Schematic of the general experimental set up for recapitulating disseminated ER+ breast tumor cells in the
750 bone marrow amidst mesenchymal stem cells (MSCs). Two different types of coculture models were used, one

751 with conditioned media (CMed; *top*) and one that involves direct contact co-culture (CC; *bottom*). MC,
752 monoculture.

753 **B**. Violin plots display the composite score of a 49-gene tumor dormancy score (DS), which was determined as
754 specific for ER+ breast cancers and previously validated in 4 independent cohorts to be predictive of tumor
755 recurrence. Statistical significance was assessed by Welch's t-test (n = 3 in each comparator group). Only
756 significant p values are displayed.

757 **C**. *Top*: Venn diagram depicts the outcome of multiple DEG analyses between different indicated comparator
758 groups that catalogs the number of suppressed genes or proteins in contact co-culture (CC) or conditioned
759 media (CMed) and the overall differential gene expression between the two cell types (MCF7 cells vs the HS5
760 bone marrow MSCs; bottom). *Bottom*: Genes/proteins that are induced in MCF7 tumor cells in coculture with
761 HS5 MSCs are binned into 3 categories (connected by arrows) based on the likely mechanisms for such
762 induction. Red = 39 uniquely upregulated transcripts in tumor cells in contact co-culture that were also identified
763 by proteomics. See also **Supplementary Figure 1** for suppression of genes and proteins upon coculture.

764 **D**. Results of a gene ontology analysis (GO Biological processes) on the transcripts and/or proteins that are
765 acquired by MCF7 cells from MSCs during contact coculture. See also **Supplementary Figure 2** for Reactome
766 pathway and GO enrichment analyses on the genes within each category in C.

767 **E**. Heatmap displays the findings of hierarchical unsupervised clustering of samples using the 39 genes
768 identified in C.

769 **F-H**. Violin plots display the composite score of the 39 genes in E in various tumor cell-MSC co-culture models,
770 e.g., MCF7↔HS5 (F), MCF7↔HS27a (G) and T47D↔HS5 (H). Statistical significance was assessed by
771 Welch's t-test (n = 3 in each comparator group). Only significant p values are displayed.

772

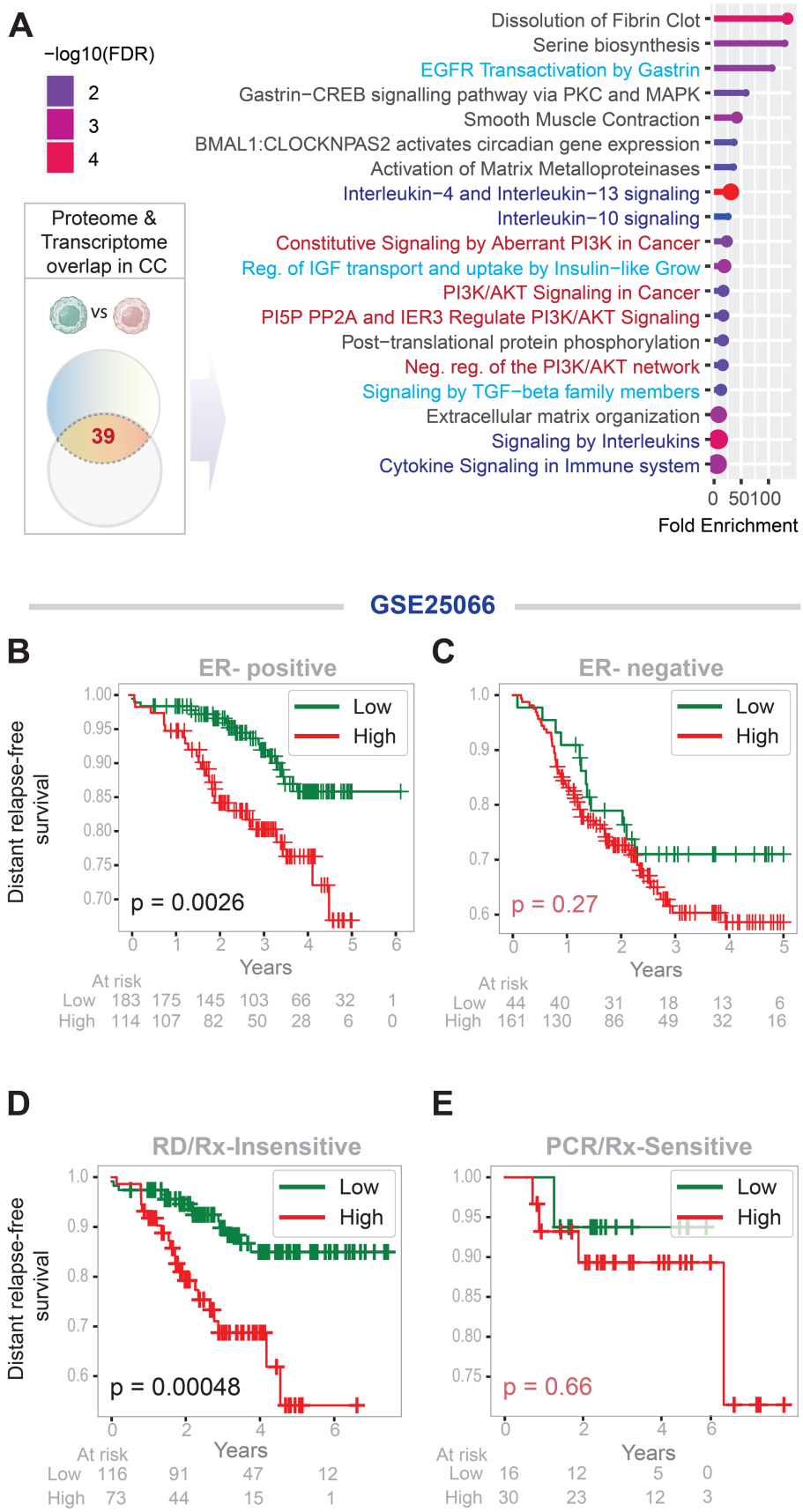

Figure 2. A contact culture signature derived from proteome-transcriptome overlap carries prognostic and predictive value in ER-positive breast cancer.

776 **A**. Reactome pathways enriched in the 39 genes identified in **Figure 1C**. The PI3K-Akt signaling pathway (red),
777 growth factor signaling pathways (teal blue) and the tolerogenic cytokine pathways (navy blue) are highlighted.

778 **B-E**. Kaplan Meier survival plots on a cohort of breast cancer patients with known outcome over time
779 (relapse/metastasis-free survival), stratified as high vs low expression of the 39-gene signature. Statistical
780 significance was assessed by Log Rank analyses.

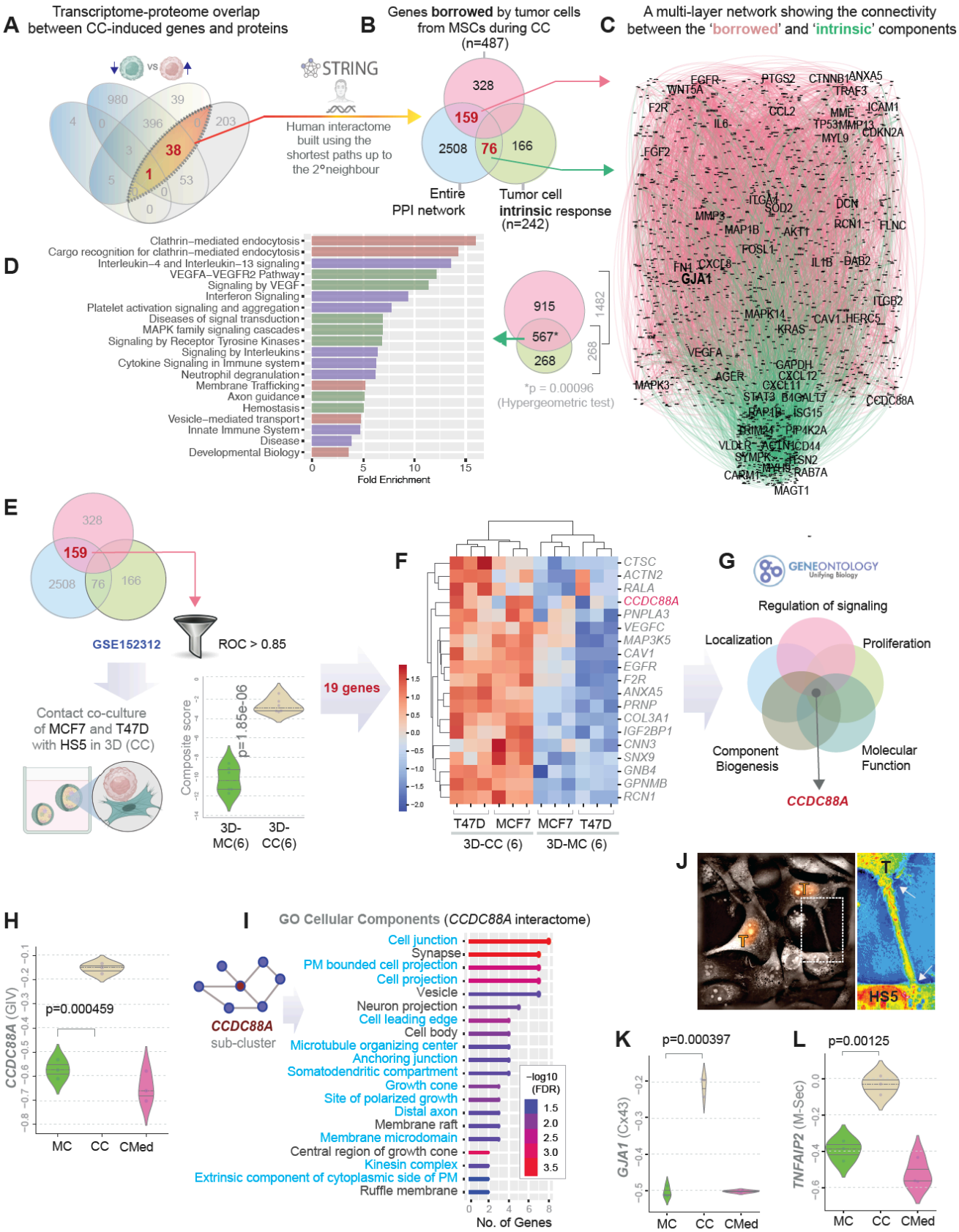

Figure 3. Network analysis pinpoints GIV as a central orchestrator of the co-culture borrowed gene signature.

A. Schematic shows the workflow for protein-protein interaction (PPI) network analysis. The 39 gene signature from Figure 1E is used as 'seeds' to build a PPI network using the STRING database (see *Methods*).

B. Venn diagram showing the overlaps between the resultant PPI network and the candidate genes/proteins that were identified in **Figure 1C** as either likely to be 'borrowed' from MSCs or upregulated as part of tumor cell's 'intrinsic' response during contact co-cultures.

C. A multi-layer PPI network shows connectivity between 'borrowed' (n = 159) and 'intrinsic' (n = 76) proteins. Key nodes in the network are labeled.

D. Reactome pathways (*left*) enriched in the 567 proteins that are shared between the borrowed and the intrinsic layers of the PPI network in C. A venn diagram (*right*) shows the total nodes in each later and the degree of overlap.

E. The 158 'borrowed' genes identified in our 2D co-culture models were further filtered using a publicly available dataset generated from 3D co-culture models wherein MCF7 and T47D cells were grown with HS5 MSCs. A threshold of ROC AUC > 0.85 led to the identification of 19 genes. A violin plot shows the composite score of the expression of 19 genes in the 3D mono (MC) vs contact (CC) cultures. Statistical significance was assessed by Welch's t-test.

F. A heatmap of z-score normalized expression of the 19 genes. MC, monoculture; CC, contact culture.

G. Venn diagram summarizes findings of gene ontology (GO) analyses, identifying *CCDC88A* as an invariant player across diverse biological processes enriched within the 19 genes.

H-I. Violin plot (H) shows the patterns of induction of *CCDC88A* in MCF7 cells when subjected to contact coculture (CC) but not when grown in conditioned media (CMed). Statistical significance was assessed by Welch's t-test. Only significant p values are displayed. Graph (I) displays the GO cellular components enriched within the *CCDC88A*/GIV-subcluster within the PPI network in C. Components highlighted in blue indicate processes that are required for enabling long-range intercellular transport via tunneling nanotubes.

J. Images obtained by inferometry microscopy of MCF7 cells (red nuclei; "T") in contact coculture with MSCs (HS5) with nanotube connecting the cells. Boxed area on left is magnified on the right. Arrows mark the two ends of the nanotube. See also **Supplementary Figure 3** for a montage of images of MCF7 cells in mono- (MC) or contact coculture (CC) with HS5 MSCs.

K-L. Violin plots show the patterns of induction of *GJA1* (K) and *TNFAIP2* (L) in MCF7 cells when subjected to contact coculture (CC) but not when grown in conditioned media (CMed). Statistical significance was assessed by Welch's t-test. Only significant p values are displayed.

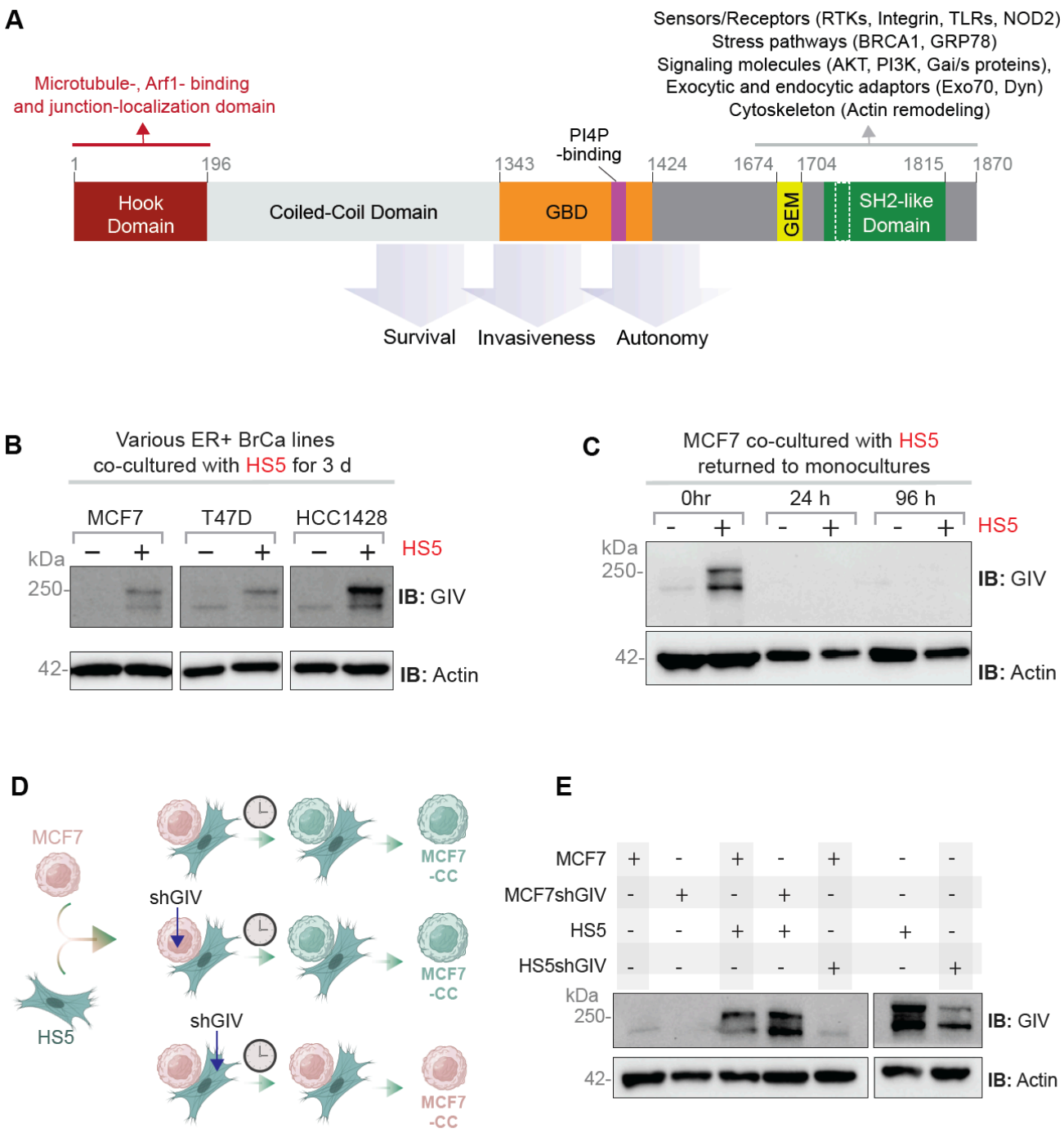

Figure 4. GIV transport from MSCs to ER+ breast cancer cells requires ongoing interactions. **A**. Schematic illustrates key functional domains of GIV. The C-terminus contains multiple short linear motifs that enable diverse tumor-promoting interactions (receptors, signaling molecules within diverse pathways, and components of membrane trafficking). GBD, G protein binding domain; GEM, guanine nucleotide exchange modulator; SH2, Src-like homology domain.

832 **B**. Equal aliquots of lysates of 3 ER+ breast cancer cells (MCF7, T47D or HCC1428) in monoculture
833 or recovered after co-culture with HS5 cells were analyzed for GIV and actin (as a loading control) by
834 immunoblotting (IB).
835 **C**. Equal aliquots of lysates of MCF7 cells prepared either immediately after recovery from co-cultures
836 with HS5 cells (0 h) or after an additional 24 or 96 h of culture after removal from HS5 contact were
837 analyzed for GIV and actin (as a loading control) by immunoblotting (IB).
838 **D-E**. Schematic (D) outlines the key manipulations (i.e., treatment with shRNA for GIV) done to either
839 MCF7 or HS5 cells in contact co-cultures. Equal aliquots of MCF7 cells recovered from the co-cultures
840 (left) or HS5 cells in monocultures were analyzed for GIV and action (loading control) by
841 immunoblotting (IB).

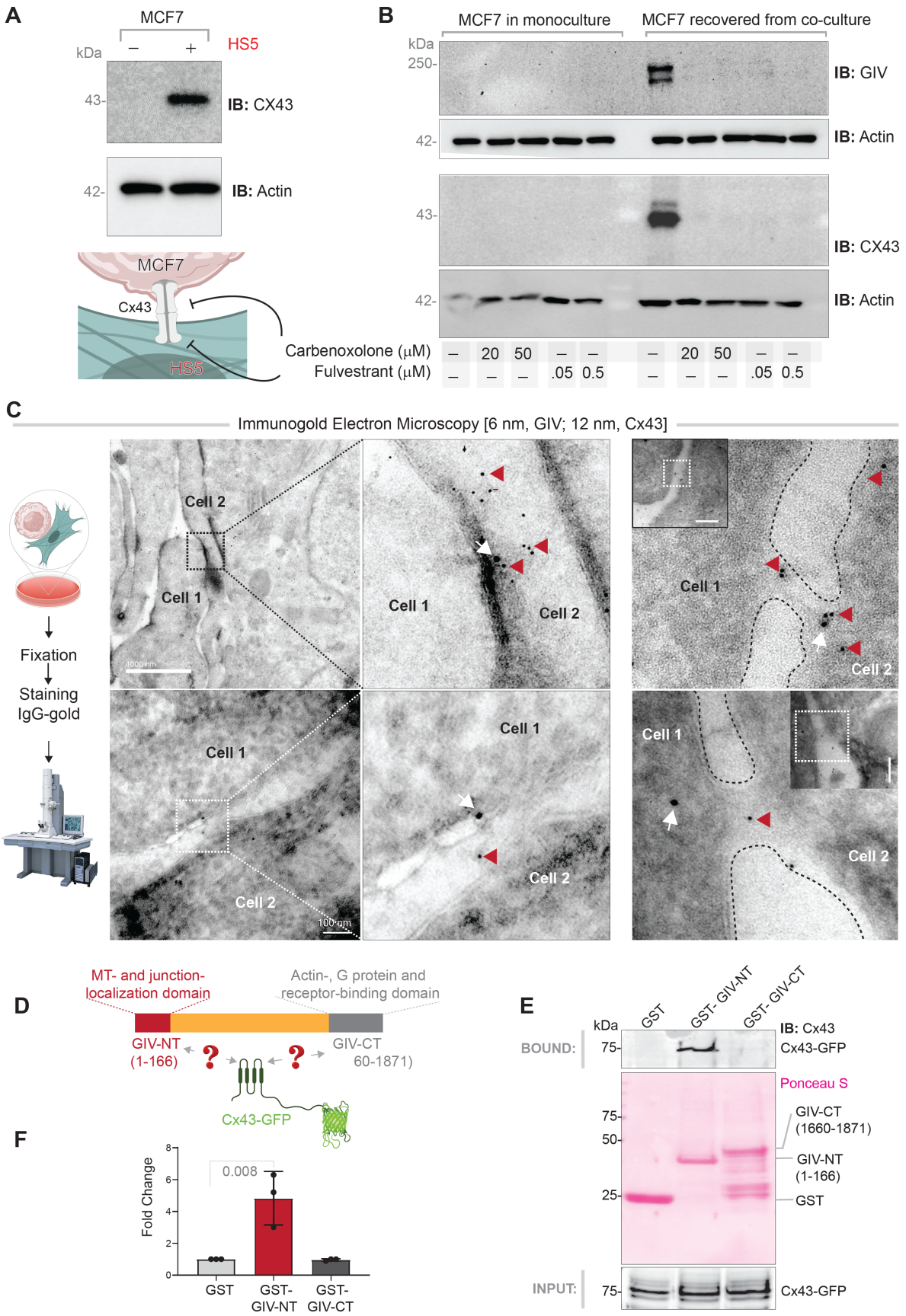

Figure 5. Cx43 and GIV interact and are co-transported through intercellular communication sites.

845 **A**. Equal aliquots of lysates of MCF7 cells in monoculture or recovered after co-culture with HS5 cells
846 were analyzed for Cx43 and actin (as a loading control) by immunoblotting (IB).
847 **B**. MCF7 cells in monoculture or in co-culture with HS5 cells were treated with the indicated
848 concentrations of Carbenoxolone or Fulvestrant prior to lysis. Equal aliquots of lysates were analyzed
849 for GIV, Cx43 or actin (the latter as a loading control) by immunoblotting (IB). See **Supplementary**
850 **Figure 5** for similar studies on HS5 monocultures.
851 **C**. Electron micrographs of immunogold stained MCF7↔HS5 contact co-cultures. Red arrowhead
852 denotes 6 nm gold particles (GIV); White arrow denotes 12 nm gold particles (Cx43). Scale bar = 100
853 μm.
854 **D-F**. Schematic of constructs (D) used in pull-down assays using recombinant GST-tagged GIV N- or
855 C-term fragments or GST alone (Neg control) proteins immobilized on glutathione beads and lysates
856 of Cos7 cells transiently expressing GFP-Cx43. Bound Cx43 was visualized by immunoblotting (E-
857 top). Equal loading of GST proteins was confirmed by Ponceau S staining (C-bottom). Bar graphs (F)
858 display the relative binding of Cx43 to various GST proteins. Data are represented as mean ± SEM
859 (n = 3); $**p=<0.01$ determined by one-way ANOVA.

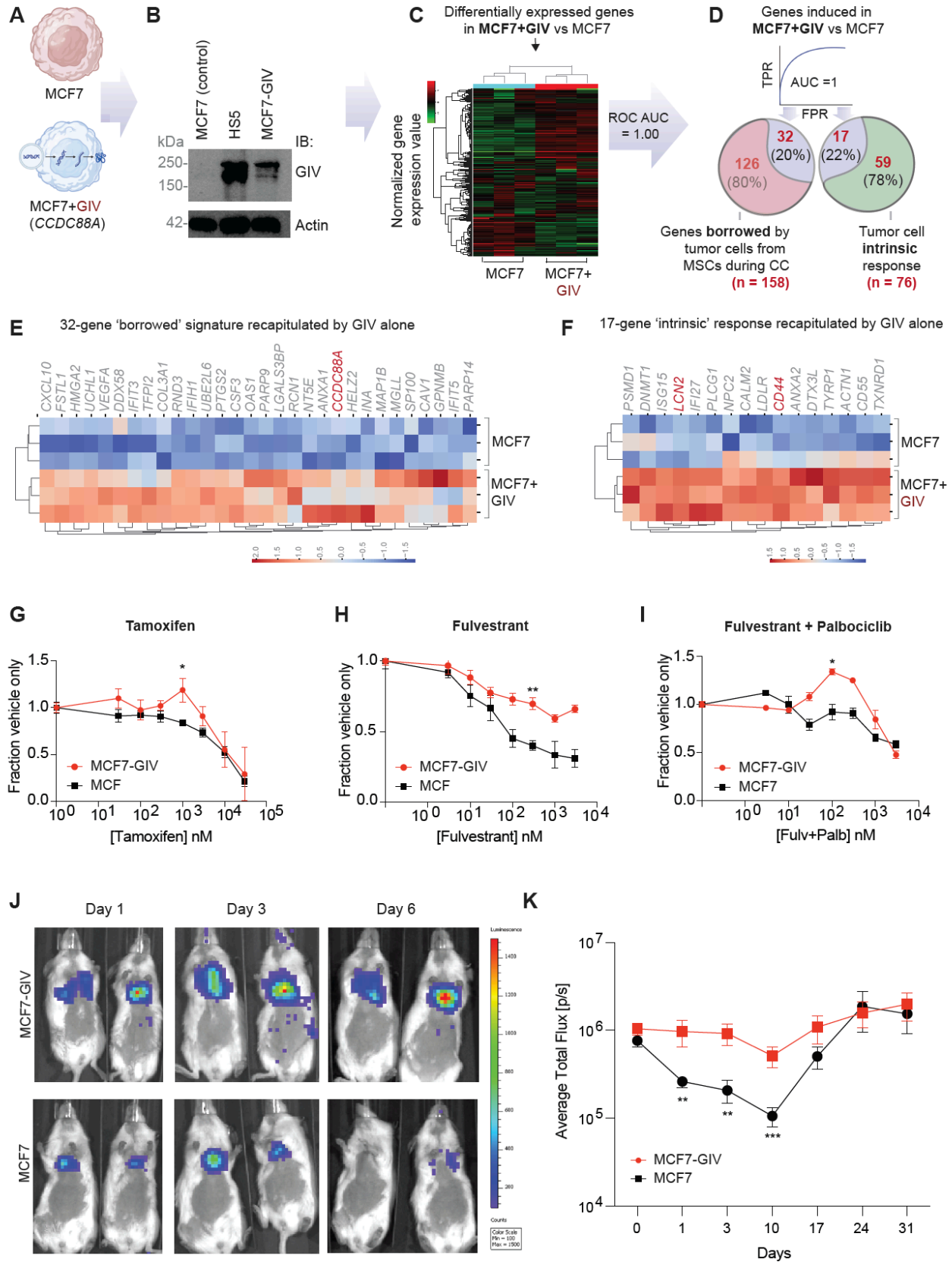

Figure 6. Expression of GIV recapitulates the MSC close contact signature;confers resistance to ER-targeted therapies; and promotes early dissemination and survival of ER+ breast cancer cells.

A. Schematic shows creation of a stable MCF7 cell population with expression of exogenous GIV (CCDC88A) by a piggyBac transposase vector.

B. Immunoblots of equal aliquots of whole cell lysates of cells in A, confirming the expression of full-length GIV.

C-D. Workflow (C) of RNA seq and normalized gene expression analysis of the cells in B, analyzed for the ability of the 'borrowed' (n=158) and 'intrinsic' (n=76) genes to perfectly classify the cells with GIV (MCF7-GIV) from those without (MCF7) (ROC-AUC 1.00). Venn diagram (D) shows the genes induced with GIV alone, as % of the total 'borrowed' and 'intrinsic' signatures.

E-F: Heatmaps display the hierarchical unsupervised clustering of MCF7 and MCF7-GIV cells by z-score normalized gene expression patterns for the subset of genes that are induced among the borrowed (E) and intrinsic (F) signatures. See also **Supplementary Figure 6** for reactome pathway analysis of these genes.

G-I. Graphs display cell viability as determined by bioluminescence when MCF7-GIV and control MCF7 cells were exposed to increasing concentrations of tamoxifen (G), fulvestrant (H), or fulvestrant and 100 nM palpociclib (I). Data are displayed after normalization to viable cells treated with vehicle only. Graphs show mean values ± SEM. *, $p < 0.05$ and **, $p < 0.01$ by AUC analysis.

J-K. Equal number (1×10^5) of MCF7-GIV or control MCF7 cells were injected into the left cardiac ventricle of 7-10-wk-old female NSG mice (n=8 per group). Representative bioluminescence images (J) of mice at day 1-, 3-, and 6-days post injection are shown. Images are displayed on a constant pseudocolor scale for photon flux with red and blue depicting high and low values, respectively. Graphs (K) show mean values ± SEM for photon flux for mice with MCF7-GIV and MCF7 cells at listed times after intracardiac injection. *, $p < 0.05$, **, $p < 0.01$, and ***, $p < 0.005$ at selected concentrations by Mann-Whitney U test.

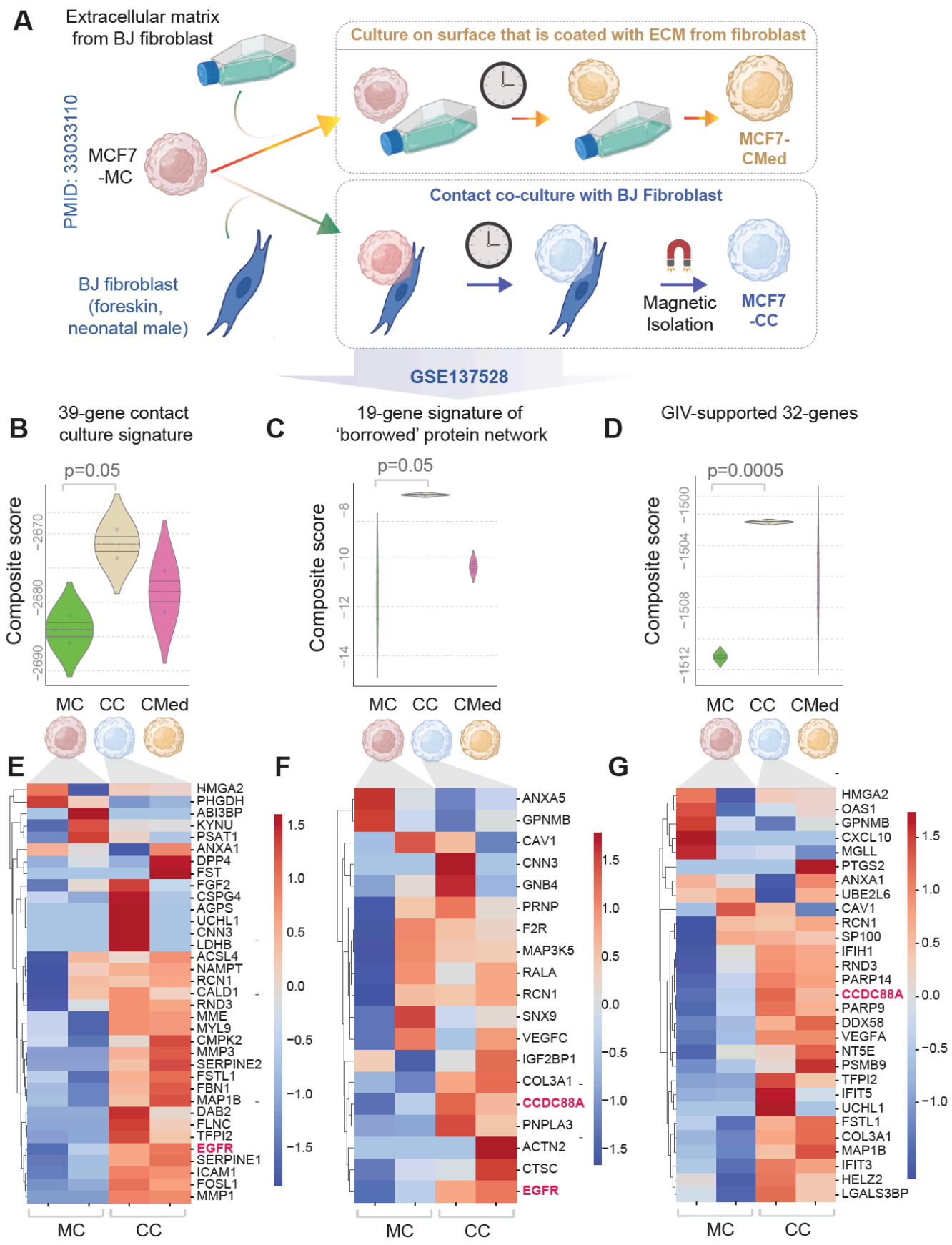

Figure 7. MCF7 cells borrow *CCDC88A* and other key genes during contact culture with fibroblasts

890 **A.** Schematic of the general experimental setup in which MCF7 cells were grown either as monoculture (MC),
891 or in direct contact cultures with BJ fibroblasts (CC) or cultured on ECM produced by the BJ fibroblasts (CMed).

892 **B-D**. Violin plots show the degrees of induction of 39-gene 2D contact culture signature (**B**), the 19-gene
893 signature of network of 'borrowed' proteins/transcripts that survived refinement through 3D contact cultures (**C**),
894 and GIV-supported 'borrowed' transcriptional program of 32 genes (as in **Fig 5D**). p-values are calculated using
895 a two-tailed t-test.

896 **E-G**. Heatmaps show the induction pattern of each gene within the signatures described in B-D. Color key
897 denotes z-score normalized counts per million (cpm).

898

899

900

901

902
903

904

905

906

907

908

909

910

911

912

913

914

915

916

917

918

919

920

921

References Cited

1. Kennecke H, Yerushalmi R, Woods R, Cheang MC, Voduc D, Speers CH, et al. Metastatic behavior of breast cancer subtypes. *J Clin Oncol.* 2010;28(20):3271-7.

2. Coleman RE, Croucher PI, Padhani AR, Clézardin P, Chow E, Fallon M, et al. Bone metastases. *Nat Rev Dis Primers.* 2020;6(1):83.

3. Weilbaecher KN, Guise TA, and McCauley LK. Cancer to bone: a fatal attraction. *Nat Rev Cancer.* 2011;11(6):411-25.

4. Pan H, Gray R, Braybrooke J, Davies C, Taylor C, McGale P, et al. 20-Year Risks of Breast-Cancer Recurrence after Stopping Endocrine Therapy at 5 Years. *N Engl J Med.* 2017;377(19):1836-46.

5. Beuzeboc P, and Scholl S. Prevention of Bone Metastases in Breast Cancer Patients. Therapeutic Perspectives. *J Clin Med.* 2014;3(2):521-36.

6. Smart E, Semina SE, and Frasor J. Update on the Role of NFκB in Promoting Aggressive Phenotypes of Estrogen Receptor-Positive Breast Cancer. *Endocrinology.* 2020;161(10).

7. Abd El-Hafeez AA, Sun N, Chakraborty A, Ear J, Roy S, Chamarthi P, et al. Regulation of DNA damage response by trimeric G-proteins. *iScience.* 2023;26(2):105973.

8. Pasquier J, Guerrouahen BS, Al Thawadi H, Ghiabi P, Maleki M, Abu-Kaoud N, et al. Preferential transfer of mitochondria from endothelial to cancer cells through tunneling nanotubes modulates chemoresistance. *J Transl Med.* 2013;11:94.

9. Imai Y, Kuba K, Rao S, Huan Y, Guo F, Guan B, et al. Angiotensin-converting enzyme 2 protects from severe acute lung failure. *Nature.* 2005;436(7047):112-6.

10. Martin FT, Dwyer RM, Kelly J, Khan S, Murphy JM, Curran C, et al. Potential role of mesenchymal stem cells (MSCs) in the breast tumour microenvironment: stimulation of epithelial to mesenchymal transition (EMT). *Breast Cancer Res Treat.* 2010;124(2):317-26.

11. Wang R, Wang X, Yin L, Chu GC, Hu P, Ou Y, et al. Breast Cancer MCF-7 Cells Acquire Heterogeneity during Successive Co-Culture with Hematopoietic and Bone Marrow-Derived Mesenchymal Stem/Stromal Cells. *Cells.* 2022;11(22).

12. Nielsen MS, Axelsen LN, Sorgen PL, Verma V, Delmar M, and Holstein-Rathlou NH. Gap junctions. *Compr Physiol.* 2012;2(3):1981-2035.

13. Wu JI, and Wang LH. Emerging roles of gap junction proteins connexins in cancer metastasis, chemoresistance and clinical application. *J Biomed Sci.* 2019;26(1):8.

14. Shiozawa Y, Pienta KJ, and Taichman RS. Hematopoietic stem cell niche is a potential therapeutic target for bone metastatic tumors. *Clin Cancer Res.* 2011;17(17):5553-8.

15. Buschhaus JM, Rajendran S, Humphries BA, Cutter AC, Muñiz AJ, Ciavattone NG, et al. Effects of iron modulation on mesenchymal stem cell-induced drug resistance in estrogen receptor-positive breast cancer. *Oncogene.* 2022;41(29):3705-18.

16. Kim RS, Avivar-Valderas A, Estrada Y, Bragado P, Sosa MS, Aguirre-Ghiso JA, et al. Dormancy signatures and metastasis in estrogen receptor positive and negative breast cancer. *PLoS One.* 2012;7(4):e35569.

962 17. Hatzis C, Pusztai L, Valero V, Booser DJ, Esserman L, Lluch A, et al. A genomic predictor of
963 response and survival following taxane-anthracycline chemotherapy for invasive breast
964 cancer. *JAMA.* 2011;305(18):1873-81.

965 18. Tishchenko A, Azorín DD, Vidal-Brime L, Muñoz MJ, Arenas PJ, Pearce C, et al. Cx43 and
966 Associated Cell Signaling Pathways Regulate Tunneling Nanotubes in Breast Cancer Cells.
967 *Cancers (Basel).* 2020;12(10).

968 19. Dhimolea E, de Matos Simoes R, Kansara D, Weng X, Sharma S, Awate P, et al. Pleiotropic
969 Mechanisms Drive Endocrine Resistance in the Three-Dimensional Bone Microenvironment.
970 *Cancer Res.* 2021;81(2):371-83.

971 20. Cordero Cervantes D, and Zurzolo C. Peering into tunneling nanotubes-The path forward.
972 *EMBO J.* 2021;40(8):e105789.

973 21. Lou E, O'Hare P, Subramanian S, and Steer CJ. Lost in translation: applying 2D intercellular
974 communication via tunneling nanotubes in cell culture to physiologically relevant 3D
975 microenvironments. *FEBS J.* 2017;284(5):699-707.

976 22. Hase K, Kimura S, Takatsu H, Ohmae M, Kawano S, Kitamura H, et al. M-Sec promotes
977 membrane nanotube formation by interacting with Ral and the exocyst complex. *Nat Cell*
978 *Biol.* 2009;11(12):1427-32.

979 23. Wittig D, Wang X, Walter C, Gerdes HH, Funk RH, and Roehlecke C. Multi-level
980 communication of human retinal pigment epithelial cells via tunneling nanotubes. *PLoS One.*
981 2012;7(3):e33195.

982 24. Warawdekar UM. An Assay to Assess Gap Junction Communication in Cell Lines. *J Biomol*
983 *Tech.* 2019;30(1):1-6.

984 25. Natsume A, Kato T, Kinjo S, Enomoto A, Toda H, Shimato S, et al. Girdin maintains the
985 stemness of glioblastoma stem cells. *Oncogene.* 2012;31(22):2715-24.

986 26. Rohena C, Kalogriopoulos N, Rajapakse N, Roy S, Lopez-Sanchez I, Ablack J, et al.
987 GIV•Kindlin Interaction Is Required for Kindlin-Mediated Integrin Recognition and Activation.
988 *iScience.* 2020;23(6):101209.

989 27. Cao F, Yang D, Tang F, Lu C, He X, Chen S, et al. Girdin Promotes Tumorigenesis and
990 Chemoresistance in Lung Adenocarcinoma by Interacting with PKM2. *Cancers (Basel).*
991 2022;14(22).

992 28. Midde K, Sun N, Rohena C, Joosen L, Dhillon H, and Ghosh P. Single-Cell Imaging of
993 Metastatic Potential of Cancer Cells. *iScience.* 2018;10:53-65.

994 29. Dunkel Y, Diao K, Aznar N, Swanson L, Liu L, Zhu W, et al. Prognostic impact of total and
995 tyrosine phosphorylated GIV/Girdin in breast cancers. *FASEB J.* 2016;30(11):3702-13.

996 30. Ghosh P. Heterotrimeric G proteins as emerging targets for network based therapy in
997 cancer: End of a long futile campaign striking heads of a Hydra. *Aging (Albany NY).*
998 2015;7(7):469-74.

999 31. Kitamura T, Asai N, Enomoto A, Maeda K, Kato T, Ishida M, et al. Regulation of VEGF-
1000 mediated angiogenesis by the Akt/PKB substrate Girdin. *Nat Cell Biol.* 2008;10(3):329-37.

1001 32. Jiang P, Enomoto A, Jijiwa M, Kato T, Hasegawa T, Ishida M, et al. An actin-binding protein
1002 Girdin regulates the motility of breast cancer cells. *Cancer Res.* 2008;68(5):1310-8.

1003 33. Ghosh P, Beas AO, Bornheimer SJ, Garcia-Marcos M, Forry EP, Johannson C, et al. A
1004 G{alpha}i-GIV molecular complex binds epidermal growth factor receptor and determines
1005 whether cells migrate or proliferate. *Mol Biol Cell.* 2010;21(13):2338-54.

1006 34. Nishimae K, Tsunoda N, Yokoyama Y, Kokuryo T, Iwakoshi A, Takahashi M, et al. The
1007 impact of Girdin expression on recurrence-free survival in patients with luminal-type breast
1008 cancer. *Breast Cancer.* 2015;22(5):445-51.

1009 35. Peng WT, Hu X, Yao L, Jiang YZ, and Shao ZM. Elevated expression of Girdin in the
1010 nucleus indicates worse prognosis for patients with estrogen receptor-positive breast cancer.
1011 *Ann Surg Oncol.* 2014;21 Suppl 4:S648-56.

1012 36. Qiao L, Sinha S, Abd El-Hafeez AA, Lo IC, Midde KK, Ngo T, et al. A circuit for secretion-
1013 coupled cellular autonomy in multicellular eukaryotic cells. *Mol Syst Biol.* 2023:e11127.

1014 37. Zurzolo C. Tunneling nanotubes: Reshaping connectivity. *Curr Opin Cell Biol.* 2021;71:139-
1015 47.

1016 38. Tsai CF, Cheng YK, Lu DY, Wang SL, Chang CN, Chang PC, et al. Inhibition of estrogen
1017 receptor reduces connexin 43 expression in breast cancers. *Toxicol Appl Pharmacol.*
1018 2018;338:182-90.

1019 39. Ren J, Wang XH, Wang GC, and Wu JH. 17β estradiol regulation of connexin 43-based gap
1020 junction and mechanosensitivity through classical estrogen receptor pathway in osteocyte-
1021 like MLO-Y4 cells. *Bone.* 2013;53(2):587-96.

1022 40. Aznar N, Patel A, Rohena CC, Dunkel Y, Joosen LP, Taupin V, et al. AMP-activated protein
1023 kinase fortifies epithelial tight junctions during energetic stress via its effector GIV/Girdin.
1024 *Elife.* 2016;5.

1025 41. Osborne CK. Tamoxifen in the treatment of breast cancer. *N Engl J Med.*
1026 1998;339(22):1609-18.

1027 42. Osborne CK, Wakeling A, and Nicholson RI. Fulvestrant: an oestrogen receptor antagonist
1028 with a novel mechanism of action. *Br J Cancer.* 2004;90 Suppl 1(Suppl 1):S2-6.

1029 43. Saptarshi Sinha AF, Kathryn E Luker, Debashis Sahoo, Barbara A Parker, Kay Yeung, Gary
1030 D Luker, Pradipta Ghosh. bioRxiv; 2022:2022.12. 02.518910.

1031 44. !!! INVALID CITATION !!! 28-30.

1032 45. Ippolito L, Morandi A, Taddei ML, Parri M, Comito G, Iscaro A, et al. Cancer-associated
1033 fibroblasts promote prostate cancer malignancy via metabolic rewiring and mitochondrial
1034 transfer. *Oncogene.* 2019;38(27):5339-55.

1035 46. DiGiacomo JW, Godet I, Trautmann-Rodriguez M, and Gilkes DM. Extracellular Matrix-
1036 Bound FGF2 Mediates Estrogen Receptor Signaling and Therapeutic Response in Breast
1037 Cancer. *Mol Cancer Res.* 2021;19(1):136-49.

1038 47. Buschhaus JM, Humphries BA, Eckley SS, Robison TH, Cutter AC, Rajendran S, et al.
1039 Targeting disseminated estrogen-receptor-positive breast cancer cells in bone marrow.
1040 *Oncogene.* 2020;39(34):5649-62.

1041 48. Davies C, Pan H, Godwin J, Gray R, Arriagada R, Raina V, et al. Long-term effects of
1042 continuing adjuvant tamoxifen to 10 years versus stopping at 5 years after diagnosis of
1043 oestrogen receptor-positive breast cancer: ATLAS, a randomised trial. *Lancet.*
1044 2013;381(9869):805-16.

1045 49. Lee SJ, Park S, Ahn HK, Yi JH, Cho EY, Sun JM, et al. Implications of bone-only
1046 metastases in breast cancer: favorable preference with excellent outcomes of hormone
1047 receptor positive breast cancer. *Cancer Res Treat.* 2011;43(2):89-95.

1048 50. Zhang XH, Giuliano M, Trivedi MV, Schiff R, and Osborne CK. Metastasis dormancy in
1049 estrogen receptor-positive breast cancer. *Clin Cancer Res.* 2013;19(23):6389-97.

1050 51. Xuan X, Tian C, Zhao M, Sun Y, and Huang C. Mesenchymal stem cells in cancer
1051 progression and anticancer therapeutic resistance. *Cancer Cell Int.* 2021;21(1):595.

1052 52. Yagi H, and Kitagawa Y. The role of mesenchymal stem cells in cancer development. *Front*
1053 *Genet.* 2013;4:261.

1054 53. !!! INVALID CITATION !!! 33.

1055 54. !!! INVALID CITATION !!! 32.

1056 55. Shee K, Yang W, Hinds JW, Hampsch RA, Varn FS, Traphagen NA, et al. Therapeutically
1057 targeting tumor microenvironment-mediated drug resistance in estrogen receptor-positive
1058 breast cancer. *J Exp Med.* 2018;215(3):895-910.

1059 56. Ahmed KA, and Xiang J. Mechanisms of cellular communication through intercellular protein
1060 transfer. *J Cell Mol Med.* 2011;15(7):1458-73.

1061 57. Vignais ML, Caicedo A, Brondello JM, and Jorgensen C. Cell Connections by Tunneling
1062 Nanotubes: Effects of Mitochondrial Trafficking on Target Cell Metabolism, Homeostasis,
1063 and Response to Therapy. *Stem Cells Int.* 2017;2017:6917941.

1064 58. Rustom A, Saffrich R, Markovic I, Walther P, and Gerdes HH. Nanotubular highways for
1065 intercellular organelle transport. *Science.* 2004;303(5660):1007-10.

1066 59. Dubois F, Bénard M, Jean-Jacques B, Schapman D, Roberge H, Lebon A, et al.
1067 Investigating Tunneling Nanotubes in Cancer Cells: Guidelines for Structural and Functional
1068 Studies through Cell Imaging. *Biomed Res Int.* 2020;2020:2701345.

1069 60. !!! INVALID CITATION !!! 42.

1070 61. Han X, and Wang X. Opportunities and Challenges in Tunneling Nanotubes Research: How
1071 Far from Clinical Application? *Int J Mol Sci.* 2021;22(5).

1072 62. Sartori-Rupp A, Cordero Cervantes D, Pepe A, Gousset K, Delage E, Corroyer-Dulmont S,
1073 et al. Correlative cryo-electron microscopy reveals the structure of TNTs in neuronal cells.
1074 *Nat Commun.* 2019;10(1):342.

1075 63. Alarcon-Martinez L, Villafranca-Baughman D, Quintero H, Kacerovsky JB, Dotigny F, Murai
1076 KK, et al. Interpericyte tunnelling nanotubes regulate neurovascular coupling. *Nature.*
1077 2020;585(7823):91-5.

1078 64. Wang X, Veruki ML, Bukoreshtliev NV, Hartveit E, and Gerdes HH. Animal cells connected
1079 by nanotubes can be electrically coupled through interposed gap-junction channels. *Proc*
1080 *Natl Acad Sci U S A.* 2010;107(40):17194-9.

1081 65. Wang X, Bukoreshtliev NV, and Gerdes HH. Developing neurons form transient nanotubes
1082 facilitating electrical coupling and calcium signaling with distant astrocytes. *PLoS One.*
1083 2012;7(10):e47429.

1084 66. Lock JT, Parker I, and Smith IF. Communication of Ca(2+) signals via tunneling membrane
1085 nanotubes is mediated by transmission of inositol trisphosphate through gap junctions. *Cell*
1086 *Calcium.* 2016;60(4):266-72.

1087 67. Okafo G, Prevedel L, and Eugenin E. Tunneling nanotubes (TNT) mediate long-range gap
1088 junctional communication: Implications for HIV cell to cell spread. *Sci Rep.* 2017;7(1):16660.

1089 68. Turos-Korgul L, Kolba MD, Chroscicki P, Zieminska A, and Piwocka K. Tunneling Nanotubes
1090 Facilitate Intercellular Protein Transfer and Cell Networks Function. *Front Cell Dev Biol.*
1091 2022;10:915117.

1092 69. Dubey GP, and Ben-Yehuda S. Intercellular nanotubes mediate bacterial communication.
1093 *Cell.* 2011;144(4):590-600.

1094 70. Pande S, Shitut S, Freund L, Westermann M, Bertels F, Colesie C, et al. Metabolic cross-
1095 feeding via intercellular nanotubes among bacteria. *Nat Commun.* 2015;6:6238.

1096 71. Koo H, Allan RN, Howlin RP, Stoodley P, and Hall-Stoodley L. Targeting microbial biofilms:
1097 current and prospective therapeutic strategies. *Nat Rev Microbiol.* 2017;15(12):740-55.

1098 72. Claessen D, Rozen DE, Kuipers OP, Søgaard-Andersen L, and van Wezel GP. Bacterial
1099 solutions to multicellularity: a tale of biofilms, filaments and fruiting bodies. *Nat Rev*
1100 *Microbiol.* 2014;12(2):115-24.

1101 73. Mandlik A, Swierczynski A, Das A, and Ton-That H. Pili in Gram-positive bacteria: assembly,
1102 involvement in colonization and biofilm development. *Trends Microbiol.* 2008;16(1):33-40.

1103 74. Preda VG, and Săndulescu O. Communication is the key: biofilms, quorum sensing,
1104 formation and prevention. *Discoveries (Craiova).* 2019;7(3):e100.

1105 75. Javid B, and Derbyshire KM. Nanotubes: shaking hands, talking, or sharing? *Front Microbiol.*
1106 2011;2:95.

1107 76. Gerdes HH, and Carvalho RN. Intercellular transfer mediated by tunneling nanotubes. *Curr*
1108 *Opin Cell Biol.* 2008;20(4):470-5.

1109 77. Lo IC, Gupta V, Midde KK, Taupin V, Lopez-Sanchez I, Kufareva I, et al. Activation of Gαi at
1110 the Golgi by GIV/Girdin imposes finiteness in Arf1 signaling. *Dev Cell.* 2015;33(2):189-203.

1111 78. Beas AO, Taupin V, Teodorof C, Nguyen LT, Garcia-Marcos M, and Farquhar MG. Gαs
1112 promotes EEA1 endosome maturation and shuts down proliferative signaling through
1113 interaction with GIV (Girdin). *Mol Biol Cell.* 2012;23(23):4623-34.

1114 79. Gupta V, Bhandari D, Leyme A, Aznar N, Midde KK, Lo IC, et al. GIV/Girdin activates Gαi
1115 and inhibits Gαs via the same motif. *Proc Natl Acad Sci U S A.* 2016;113(39):E5721-30.

1116 80. Garcia-Marcos M, Ear J, Farquhar MG, and Ghosh P. A GDI (AGS3) and a GEF (GIV)
1117 regulate autophagy by balancing G protein activity and growth factor signals. *Mol Biol Cell.*
1118 2011;22(5):673-86.

1119 81. Ghosh P, and Mullick M. Building unconventional G protein-coupled receptors, one block at
1120 a time. *Trends Pharmacol Sci.* 2021;42(7):514-7.

1121 82. Yamamura Y, Asai N, Enomoto A, Kato T, Mii S, Kondo Y, et al. Akt-Girdin signaling in
1122 cancer-associated fibroblasts contributes to tumor progression. *Cancer Res.*
1123 2015;75(5):813-23.

1124 83. Sandipan Dasgupta 1 DYD, Gal Haimovich 1,4 , Emanuel Wyler 2 , Tsviya
1125 Olender 1 , Robert H. Singer 3 , Markus Landthaler 2 , and Jeffrey E. Gerst.

1126 84. Dunkel Y, Ong A, Notani D, Mittal Y, Lam M, Mi X, et al. STAT3 protein up-regulates Gα-
1127 interacting vesicle-associated protein (GIV)/Girdin expression, and GIV enhances STAT3
1128 activation in a positive feedback loop during wound healing and tumor invasion/metastasis. *J*
1129 *Biol Chem.* 2012;287(50):41667-83.

1130 85. Fiori ME, Di Franco S, Villanova L, Bianca P, Stassi G, and De Maria R. Cancer-associated
1131 fibroblasts as abettors of tumor progression at the crossroads of EMT and therapy
1132 resistance. *Mol Cancer.* 2019;18(1):70.

1133 86. Cavnar SP, Rickelmann AD, Meguiar KF, Xiao A, Dosch J, Leung BM, et al. Modeling
1134 selective elimination of quiescent cancer cells from bone marrow. *Neoplasia.*
1135 2015;17(8):625-33.

1136 87. Smith MC, Luker KE, Garbow JR, Prior JL, Jackson E, Piwnica-Worms D, et al. CXCR4
1137 regulates growth of both primary and metastatic breast cancer. *Cancer Res.*
1138 2004;64(23):8604-12.

1139 88. Cavnar SP, Xiao A, Gibbons AE, Rickelmann AD, Neely T, Luker KE, et al. Imaging
1140 Sensitivity of Quiescent Cancer Cells to Metabolic Perturbations in Bone Marrow Spheroids.
1141 *Tomography.* 2016;2(2):146-57.

1142 89. Buschhaus JM, Rajendran S, Chen S, Wharram BL, Bevoor AS, Cutter AC, et al. Bone
1143 marrow mesenchymal stem cells induce metabolic plasticity in estrogen receptor-positive
1144 breast cancer. *Mol Cancer Res.* 2023.

1145 90. Buschhaus Johanna M, Rajendran S, Humphries B, Cutter A, Ciavattone N, Buschhaus A,
1146 et al. Effects of iron modulation on mesenchymal stem cell-induced drug resistance in
1147 estrogen-receptor-positive breast cancer. 2022.

1148 91. Perez-Riverol Y, Bai J, Bandla C, García-Seisdedos D, Hewapathirana S, Kamatchinathan
1149 S, et al. The PRIDE database resources in 2022: a hub for mass spectrometry-based
1150 proteomics evidences. *Nucleic Acids Res.* 2022;50(D1):D543-D52.

1151 92. Sahoo D, Dill DL, Tibshirani R, and Plevritis SK. Extracting binary signals from microarray
1152 time-course data. *Nucleic Acids Res.* 2007;35(11):3705-12.

1153 93. Sahoo D, Swanson L, Sayed IM, Katkar GD, Ibeawuchi SR, Mittal Y, et al. Artificial
1154 intelligence guided discovery of a barrier-protective therapy in inflammatory bowel disease.
1155 *Nat Commun.* 2021;12(1):4246.

1156 94. Fabregat A, Jupe S, Matthews L, Sidiropoulos K, Gillespie M, Garapati P, et al. The
1157 Reactome Pathway Knowledgebase. *Nucleic Acids Res.* 2018;46(D1):D649-D55.

1158 95. Stout RF, Snapp EL, and Spray DC. Connexin Type and Fluorescent Protein Fusion Tag
1159 Determine Structural Stability of Gap Junction Plaques. *J Biol Chem.* 2015;290(39):23497-
1160 514.

1161 96. Ear J, Abd El-Hafeez AA, Roy S, Ngo T, Rajapakse N, Choi J, et al. A long isoform of
1162 GIV/Girdin contains a PDZ-binding module that regulates localization and G-protein binding.
1163 *J Biol Chem.* 2021;296:100493.

1164 97. Boussif O, Lezoualc'h F, Zanta MA, Mergny MD, Scherman D, Demeneix B, et al. A versatile
1165 vector for gene and oligonucleotide transfer into cells in culture and in vivo:
1166 polyethylenimine. *Proc Natl Acad Sci U S A.* 1995;92(16):7297-301.

1167